A shielded irradiation assay to investigate mechanisms of *in vivo* stem cell migration in planarians.

Prasad Abnave[1], Ellen Aboukhatwa[1], Nobuyoshi Kosaka[1], James Thompson[2], Mark A. Hill[2], A. Aziz Aboobaker[1]*

1. Department of Zoology, Tinbergen Building, South Parks Road, University of Oxford, Oxford OX1 3PS, United Kingdom

2. CRUK/MRC Oxford Institute for Radiation Oncology, ORCRB Roosevelt Drive, University of Oxford, Oxford OX3 7DQ, United Kingdom

correspondence: Aziz.Aboobaker@zoo.ox.ac.uk

Abstract

The migration of stem cells is an essential process underpinning the physiology of all metazoan animals. In order for tissues to be maintained, homeostatic signaling mechanisms must allow stem cells or their progeny to arrive at the correct position and differentiate into replacement cells. This need is even more acute after tissue damage by wounding or pathogenic infections. Inappropriate migration of tumorigenic cancer stem cells and their progeny in adults also underpins the formation of metastases. Despite this, few mechanistic studies address stem cell migration during repair after injury in adult tissues. Here we present a shielded X-ray irradiation assay that allows us to watch cell migration in the highly regenerative planarian model system. We demonstrate that we can carefully observe migratory behavior and reveal new phenomena concerning migration, not previously observed in planarians. These include observation of cell migration specifically in an anterior direction in the absence of injury. We demonstrate that this homeostatic migration requires the polarity determinant *notum.* The morphology and distribution of migrating stem cells implicates mechanisms associated with epithelial to mesenchymal transition (EMT). In agreement with this we find that a planarian Snail family transcription factor is necessary for stem cell and stem cell progeny migration to wound sites and for the establishment of migratory morphology. Overall our data establish planarians as a suitable model for further in depth study of cell migration, with the potential to yield novel insights relevant to human biology including hyperplasia during cancer progression.

Introduction

Regeneration and tissue homeostasis in multicellular animals are a result of the activity of their stem cells. Most animal adult life histories include some potential to regenerate lost cells, tissues and organs but the efficiency and extent of the regenerative process varies greatly amongst species. Many basal invertebrates like cnidarians, flatworms and annelids are capable of whole body regeneration and some of these are now experimentally tractable model organisms for studying regeneration and homeostasis[1-2]. Studies of invertebrate stem cells that contribute to regeneration and homeostasis inform us about the origins of key stem cell properties, such as the abilities to self-renew, produce progeny that interpret positional information to differentiate and form the cells necessary for tissue and organ homeostasis and regeneration[1-2]. In planarians, for example, adult stem cells collectively called neoblasts fuel regeneration and are now known include both pluripotent stem cells and distinct classes of lineage committed cycling cells[3–4].

So far few studies in regenerative models have investigated stem cell and stem cell progeny migration, even though migration to site of injury or homeostatic migration is a key stem cell activity for regeneration and repair and has important biomedical applications[5–7]. The over-activity of migratory mechanisms is a feature of tumor tissue invasion and the pathology caused by cancers[8]. More recently it has become clear that stem cell migration is tied to other key features of stem cell biology such as potency, differentiation and genome stability[9]. Thus defects in this key part of stem cell function are likely to contribute to many age related processes leading to disease, and these links remain poorly described, particularly *in vivo*[10]. Many studies have revealed common mechanisms driving cell migration in different contexts[10–13]. However, studying cell migration *in vivo* is technically challenging, and simple model systems amenable to functional study may have a lot to offer. For example, *in vivo* studies in both *Drosophila* and *C. elegans* during embryogenesis and larval development have proved very useful for unveiling fundamental molecular mechanisms also used by vertebrates[14,5,15–17]. The planarian system, in which stem cell and their progeny can be easily identified and studied, is another potentially tractable system[18]. Here we used the model planarian *Schmidtea mediterranea* to study cell migration during regeneration and normal tissue homeostasis. So far most studies in *Schmidtea* have focused on how stem cell self-renewal, division and differentiation are controlled or how more broadly tissue polarity and position are controlled[19–22,4,23]. Less focus has been given to cell migration, although it is an

65 essential component of a successful regenerative outcome. In this work we perfect an assay to
66 allow precise observation of cell migration and describe novel phenomena regarding cell
67 migration in the planarian system, including cell migration in the absence of wounding. Our
68 work uncovers an intricate relationship between known stem cell and stem cell progeny
69 lineages and the order of cell migration, suggesting a close relationship between the
70 migration, proliferation and differentiation processes. We also show that RNAi can be
71 efficiently employed with our migration assay. This allowed us to demonstrated clearly the
72 requirements for Snail family transcription factor and a matrix-metalloprotease (MMP) for
73 normal cell migration. Finally, we show that the anterior migration of stem cell and stem cell
74 progeny in the absence of wounding relies on the previously described polarity protein *Notum*.
75 Our work establishes the possibility of using *Schmidtea* as a highly effective model system to
76 study adult stem cell migration in a regenerative context.

77 **Results**

78 **Establishment of an X-ray shielded method for tracking stem cell migration**

79 Classic research using planarians nearly a century ago established that planarian regenerative
80 properties were sensitive to high doses of ionizing radiation and later this was attributed to the
81 fact that proliferative stem cells, called neoblasts, were killed by the irradiation[25]. Partially
82 exposing planarians to ionizing radiation, through use of a lead shield, was shown to slow
83 down regenerative ability and suggested the possibility that neoblasts were potentially able to
84 move to exposed regions and restore regenerative ability[26]. Recently established methods for
85 tracking cell migration in planarians have either revisited shielding some portion of the stem
86 cell population from irradiation or involved transplanting tissue with stem cells into lethally
87 irradiated hosts[7,27]. These methods clearly showed movement of proliferative stem cells and
88 stem cell progeny[7,27]. However, these approaches have some technical features that may have
89 made the study of gene function challenging. Firstly, both approaches as published required
90 the use of large animals. Larger planarians require some special attention for culturing and
91 can be more difficult to work with. For example, in situ hybridization approaches are less
92 effective in larger animals[28]. Secondly, shielding as well as transplanting individual worms
93 becomes labor intensive if performed on larger numbers of worms required for functional
94 genomic approaches, which needs consistent treatment. With this in mind we set out with the
95 goal of adapting the classical lead shielding approach and establishing an assay to tackle these
96 existing technical issues, making it more practical to exploit *Schmidtea* to study the molecular

control of cell migration. Specifically, we wished to be able to use irradiation to generate a much smaller shielded region to allow the use of smaller worms and at the same time be able to perform consistent experiments across a larger number of animals, rather than shielding animals individually.

We designed an irradiation technique in which multiple animals can be uniformly irradiated with X-rays, apart from a thin strip in a predetermined position along its length. This is achieved by placing the animals directly above a 0.8 mm strip of lead (6.1 mm thick), to significantly attenuate the X-rays in the region just above lead (Supplementary Figure 1A and 1B, Figure 1A-C) to less than 5% (in the central 0.5mm region) of the dose in the rest of the animal (Supplementary Figure 1C).

Our final working version of the apparatus is conveniently designed to fit a standard 60 mm petri dish, with the lead shield lying below the diameter. Anaesthetized planarians are aligned across the diameter in preparation for X-ray exposure (Figure 1 A-C). We could then expose up to 20 ~3-5mm long worms simultaneously to a normally lethal 30 Gy X-ray dose in a 1 min 18 sec exposure, with the shielded region receiving <1.5 Gy. This allows for some precision in controlling the position of a surviving band of stem cells (Figure 1D and E). Looking at animals with the shield positioned centrally along the anterior to posterior (AP) axis we performed whole mount fluorescent in situ hybridization (WFISH) to assay the effectiveness of the shield. With the *smedwi-1* stem cell marker we confirmed that all stem cells (*smedwi-1*$^+$) outside the shielded region disappear by 24 hours post irradiation (pi) and with the early epidermal lineage marker NB21.11e, that stem cell progeny (*prog1*$^+$) outside the shielded region have differentiated by 4 days pi (Figure 1E and F). We observed that cells within the shield have a density equivalent to that in wild type animals not subjected to shielded irradiation, suggesting that the shield is effective at protecting cells (Figure 1E and F and see later for quantification). We also noted that there is no cell migration from the shielded region during this time (Figure 1E and F). We observed that a few *smedwi-1*$^+$ cells very close to the shield boundary survived beyond 24 hours, but that these were not detected by 4 days (Figure 1F). We hypothesize that these cells receive an attenuated dose of ionizing radiation that is not lethal within 24 hours but nonetheless they are not competent to self-renew, instead they die or differentiate at later time points. These data established that any observation of migrating stem cells and stem cell progeny should ideally occur after 4 days pi, and that with an AP shield centrally positioned cells do not migrate in the absence of injury.

129 In summary our X-ray shielded assay system allows for convenient and precise observation of
130 stem cell and stem cell progeny behavior over time post-irradiation, and in animals suitable
131 for functional studies.

132 **Anterior migration of stem cells and stem cell progeny in the absence of wounding**

133 We next decided to use our system to describe the movement of stem cells and stem cell
134 progeny in worms after X-ray shielded irradiation to confirm and add to previous
135 observations. The cycling stem cells in *Schmidtea* are normally present throughout the body
136 but absent from in front of the photoreceptors and the centrally positioned pharynx and are not
137 detectable within early regenerative blastema (Supplementary Figure 2A and B). These facts
138 mean that in normal animals i) stem cells would not normally have far to migrate during
139 normal homeostasis or regeneration as they will always be relatively close to where they are
140 required, except for the anterior region and the pharynx, ii) in the context of early
141 regeneration stem cell progeny migrate to establish the blastema tissue before stem cells, and
142 iii) at least for the pharynx and the most anterior tissue, homeostasis is achieved by migration
143 of post-mitotic stem cell progeny, not stem cells. Together this leads us to expect stem cell
144 progeny to have migratory properties that are distinct from cycling stem cells, in particular
145 that should be active during normal homeostasis and may respond earlier to wound signals.
146 We hypothesized therefore that observations within the context of our X-ray shielded assay
147 would be consistent with these cell behaviors.

148 To begin, we shielded animals of equal size at different positions along the AP axis and
149 irradiated them (Figure 2A). When the shield was placed in the posterior region of worms we
150 observed tissue death and regression from the anterior towards the shield (Figure 2B).
151 Subsequently, we observed blastema formation and normal regeneration that took up to 50
152 days pi (Figure 2C). Using WFISH we were able to observe that stem cells and stem cell
153 progeny did not migrate until anterior tissue had regressed to close to the wound site (Figure
154 2D). When animals where shielded in mid body regions with top of the shield level with the
155 most anterior region of the pharynx we often observed regression from the anterior and
156 posterior (Figure 2E). Again we subsequently observed blastema formation and regeneration
157 that took up to 45 days (Figure 2F). In contrast, for animals where the posterior of the shield
158 was positioned level with the posterior of the pharynx we observed that worms often
159 displayed posterior regression and not anterior regression (Figure 2H and I). In these animals
160 the head never regressed with the tail regressing and then regenerating normally over several

161 weeks (Figure 2I). These results suggest that leaving a stripe of more anteriorly positioned
162 cells was somehow sufficient to maintain anterior tissues.

163 To investigate this further we irradiated animals with shields positioned at different points and
164 performed WFISH to observe stem cells and stem cell progeny at different time points post
165 irradiation. We observed that depending on the distance of the fixed posterior boundary of the
166 shield from the anterior tip of animals we were able to observe migration of cells towards the
167 anterior in the absence of wounding (Figure 2J and K). In shields placed more posteriorly we
168 did not observe cell migration until homeostasis of anterior tissues had failed and/or tissue
169 had regressed towards the shield (Figure 2D and G).

170 These data add to previous work that described that migration only occurs after wounding or
171 when tissue homeostasis fails and tissue regression towards the wound occurs[7]. We find that
172 when stem cells and stem cell progeny are in the pre-pharyngeal anterior region they can
173 migrate to the anterior in the absence of wounding and before tissue homeostasis fails. This
174 migratory activity restores the normal distribution of both progeny and stem cells and
175 suggests the presence of anterior signals that can call stem cell and stem cell progeny into the
176 brain and anterior structures over a restricted range. To quantify this effect we measured the
177 anterior migration of stem cells and *prog1*$^{+}$ cells from different starting distances (dependent
178 on shield position) from the anterior tip of animals that were ~3 mm in length. We found that
179 at starting distances up to ~1.2 mm from the anterior tip stem cell progeny and stem cells
180 migrated robustly, but above this almost no migration was observed (Figure 2K). These
181 observations suggest that an anterior signal exists for encouraging cell migration in intact
182 animals that's acts over the brain region (Figure 2L). In normal animals this may be
183 responsible for ensuring homeostasis of the brain and anterior regions, which are devoid of
184 conspicuous numbers of cycling stem cells. Recently, a *Notum/Wnt11-6* dependent signaling
185 mechanism for regulating brain size has been described as responsible for the recruitment of
186 stem cells and stem cell progeny[29]. This regulatory circuit represents a candidate system for
187 regulating the anterior migration that we observe in the absence of wounding. When cells in
188 the shield are outside the range of this signal they do not migrate until tissue homeostasis fails
189 and presumably signals emanating from regressing tissues are within range to trigger
190 migration (Figure 2D).

191 **General features of planarian cell migration after wounding**

192 We shielded animals over the pharynx and made anterior wounds. We used the lack of
193 posterior migration in this experimental design to facilitate measurements of cell migration
194 distances over time (Figure 3A). Quantifying *smedwi-1*$^+$ stem cells, *prog1*$^+$ stem cell progeny
195 and mitotic cells in the migratory region just anterior to the pharynx allowed us to develop a
196 detailed overview of the migration process (Figure 3B-E).

197 While we observed that the most advanced *smedwi-1*$^+$ cells can match the extent of migration
198 of the most advanced *prog1*$^+$ cells, we also noticed that many more *prog1*$^+$ cells enter the
199 migratory region than *smedwi-1*$^+$ cells over the first 4 days post amputation (pa). (Figure 3B-
200 D). This observations suggest that stem cell progeny react *en masse* to a wound derived signal
201 and stem cells follow, either independently in response to the wound signal or because they
202 somehow sense the migration of *prog1*$^+$ cells and follow, or some combination of both. By 7
203 days pa normal homeostatic ratios of stem cells and stem cell progeny present in the shielded
204 region and unexposed animals are also restored in the migratory region just anterior to the
205 shield (Figure 3D). We observed cells in M-phase within the field of migrating cells, the
206 numbers of which increased in proportion with the numbers of migrating *smedwi-1*$^+$ stem
207 cells over time (Supplementary Figure 3A, B and Figure 3E). This pattern of stem cell
208 proliferation in the migratory region is consistent with the homeostatic ratio of stem cells and
209 stem cell progeny being restored by symmetric stem cell divisions as well as by further
210 migration from the shield (Figure 3D). From this data we deduce that increases in number of
211 both stem cell and stem cell progeny outside of the shielded region are fuelled initially by
212 migration but then by both further migration and proliferation of stem cells.

213 Stem cell progeny that reach the wound site at 10 days pa can only have arisen from
214 asymmetric divisions of stem cells as recently as 6 days pa as this is the maximum time before
215 that differentiate and stop expressing the *prog-1* marker. Given the maximum migration
216 speeds observed over the first 4 days pa (Figure 3C) these cells must be the progeny of stem
217 cells that have already migrated. Taken together, this data suggests that migrating *smedwi-1*$^+$
218 cells undergo both symmetric and asymmetric cell divisions that increase both the number of
219 *smedwi-1*$^+$ cells and *prog1*$^+$ cells, importantly providing a source of stem cell progeny that do
220 not derive from the shielded region. We note the remarkable similarity in the dynamics that
221 we observe bare to normal regeneration after amputation, where stem cell progeny form the
222 initial regeneration blastema with stem cells only following later.

223 We also wished to know how precise the homing of migrating cells to wounds could be. To
224 investigate this we performed single 'poke' wounds at the midline or notches confined to one
225 side of the animal (Supplementary Figure 3C and D). We observed that even these small
226 injuries that were in relatively close proximity incited distinct migratory responses around
227 each wound site, indicating that migrating cells home with precision to injuries
228 (Supplementary Figure 3C and D). We note that despite the absence of stem cells and progeny
229 in the anterior tissue field migrating stem cell progeny only migrated and collected around the
230 wound, suggesting they may sense the rest of the 'blank canvas' at early time points and the
231 wound signal takes precedence. We also observed as a general feature of migration towards
232 the wound site that dorsal *prog1*$^{+}$ cells appear to migrate more rapidly than ventral cells to the
233 same wound (Supplementary Figure 3E, F), and that dorsal *smedwi-1*$^{+}$ cells migrate centrally
234 while ventral stem cells migrate across the width of animals (Supplementary Figure 3G).

235 **Migrating planarian cells have a distinct morphology of extended cell processes**

236 We next decided to investigate the migrating cells themselves in more detail, to see if we
237 could understand more about how they move in *Schmidtea*. We imaged migrating cells after
238 wounding and compared this to cells remaining in the shielded region that were static. We
239 observed a significantly higher frequency of individual stem cells and stem cell progeny with
240 extended cell processes in migratory regions of injured animals than in animals that were
241 uninjured or for cells in the shielded region were not actively migrating (Figure 4A-D, see
242 Supplementary Figure 4A-D for examples of cells with and without processes). We did not
243 observe any connection or alignment between cells with extended processes demonstrating
244 individual cells migrate independently with mesenchymal cell like morphology rather than
245 any mechanism involving collective movement of cells requiring cell-cell junction contact.
246 This observation suggests that cell migration may involve cellular mechanisms similar to
247 those used during classical epithelial to mesenchymal transition (EMT). While net movement
248 of cells is towards the wound site, we note that cell processes can extend in all directions, not
249 just towards the wound (Figure 4C and E-H).

250 **The arrangement of cell migration toward wounds recapitulates known cell lineages**

251 Ongoing planarian research has begun to reveal the details of planarian stem cell and progeny
252 lineages, in particular uncovering heterogeneity of gene expression in the cycling cell fraction
253 that very likely represents underlying functional heterogeneity and lineage commitment[4].

254 Thus, we can use the cell type markers from these studies now that allows us to label different
255 populations of cycling cells and stem cell progeny, particularly for the epidermal lineage. We
256 know that some *smedwi-1*$^{+}$ stem cells shows elevated expression of *Smed-soxP-1*, *Smed-soxP-*
257 *2* (called sigma-class neoblasts) and give rise to another class of *smedwi-1*$^{+}$ cells that express
258 discrete set of genes like *Smed-zfp-1*, *Smed-fgfr-1*, *Smed-soxP-3*, and *Smed-egr-1* (called zeta-
259 class neoblasts), these in turn produce *prog1*$^{+}$ cells that eventually begin to express the later
260 progeny marker *agat-1*, at least some of which go on to form epidermal cells[4].

261 We investigated the expression of these markers in migrating cells using a series of double
262 WFISH experiments. These allowed us to measure the extent of migration of each of these
263 cell types to begin to understand the relationship between migration and differentiation. Using
264 this approach we are able to demonstrate a trend between the extent of migration and the
265 extent of cellular differentiation (Figure 5A-J). This suggests that these processes are linked
266 by underlying mechanisms and that as stem cells migrate they divide to give daughter cells
267 that migrate and differentiate. We see a clear trend that migration distance increases with later
268 markers of the epidermal lineage, in particular we see a significant difference between
269 *smedwi-1* positive zeta class cells (zeta-class neoblasts) and *smedwi-1* negative zeta class
270 cells, which is a likely demarcation between migrating cycling cells and non-cycling progeny
271 (Figure 5G, H, K). We note that, this pattern recapitulates what is observed in the early
272 regeneration blastema, where cycling cells do not enter until later after fully differentiated
273 structures start to form.

274 **RNAi in the context of shielded irradiation reveal a matrix metalloprotease and a snail**
275 **transcription factor are required for cell migration to wound sites.**

276 Having provided a detailed description of cell migration in *Schmidtea* and uncovered
277 previously un-described behaviors we next wished to test if we could study gene function in
278 the context of migration. Previous research had attempted to implicate a *Smed-MMPa*
279 (*MMPa*), one of four matrix metalloprotease enzymes identifiable in the *Schmidtea* genome,
280 as having possible role in cell migration[30]. We decided to look at the function of this gene in
281 the context of our migration assay. We first performed RNAi in the context of normal
282 regeneration and amputation, and observed that *MMPa(RNAi)* animals showed regeneration
283 defects as previously described, with failure to correctly regenerate anterior or posterior
284 tissues (Supplementary Figure 5A)[30]. We then performed RNAi and amputation in the context
285 of our assay and observed that anterior tissues regressed and that regeneration subsequently

286 failed (Supplementary Figure 5B). We used WFISH to monitor the movement of *smedwi-1*$^{+}$
287 stem cells and *prog1*$^{+}$ stem cell progeny after *MMPa(RNAi)*, and observed very little
288 migration of cells compared to control *GFP(RNAi)* worms (Figure 6A, D, J). Additionally we
289 measured the morphology of stem cells and stem cell progeny and observed greatly reduced
290 numbers of cells with extended processes compared to migrating cells in the *GFP(RNAi)*
291 control animals (Figure 6B, C, E, F and K). These results confirm that this matrix
292 metalloprotease enzyme is required to facilitate cell migration in planarians and demonstrate
293 the potential utility of our assay in generating insights into how stem cell migration is
294 controlled.

295 We next considered if we could establish a broad comparative context for the control between
296 cell migration in planarians and migration in other systems including mammals. Our
297 observation that cells appear to migrate individually using cell extensions to likely interact
298 with the extracellular matrix and neighboring cells suggested that these cells may use similar
299 mechanisms to those attributed to EMT[31]. In different model organisms EMT during
300 embryogenesis and during the progression of tumors requires the activity of Snail family
301 transcription factors[32–34]. We decided to test whether any planarian snail transcription factors
302 could be involved in cell migration. Previously a snail family transcription factor, *Smed-snail*
303 (*snail*) has been reported as being expressed in collagen positive muscle cells, in very small
304 percentage of G2/M stem cells before wounding and ~35% of G2/M cells after wounding[35].
305 To our knowledge no phenotype has been reported for a snail family gene in planarians and
306 when we performed *snail(RNAi)* with a standard regenerative assay we observed no
307 phenotype, and all animals regenerated normally (Supplementary Figure 5A). When we
308 performed *snail(RNAi)* in the context of our migration assay animals failed to regenerate
309 suggesting a defect in cell migration (Supplementary Figure 5B). Using WFISH experiments
310 we observed a clear decrease in the extent of cell migration compared to *GFP(RNAi)* animals
311 (Figure 6A, G and J). This defect in migration of both stem cells and stem cell progeny was
312 accompanied a decrease in the number of cells with cell extensions, suggesting that migratory
313 mechanisms are effected by *snail(RNAi)* (Figure 6B, C, H, I and K). Finally we note that in
314 *snail(RNAi)* animals the normal ratio of stem cells to stem cell progeny is not restored in the
315 migratory region (Figure 6L). These defects relative to controls suggest that a snail
316 transcription factor in planarians may have a conserved role in regulating cell migration. Our
317 data suggest that our assay now facilitates the use of planarians as a model system to study the
318 migration of cells during regeneration and that many processes are likely to conserved with

319 other animals, potentially including those processes that contribute to tumor development
320 during cancer progression.

321 ***Notum* is required for anterior cell migration in intact animals, but not after wounding.**

322 Having established that our assay allows the observation of migratory stem cell behavior, can
323 be combined the application of RNAi and that the function of *snail*, a key regulator of
324 migration in many contexts, is conserved we next turned our attention to potential migratory
325 signals. Our experiments have established, in agreement with previous work, that wounding at
326 a distance triggers migration of stem cells and stem cell progeny. In addition we have shown
327 that in the absence of wounding, cells close to the anterior can still migrate into anterior
328 regions. By analogy with other systems there are clearly a large number of conserved
329 candidate pathways that could be involved in propagating the wound signal to allow migration
330 or signals involved in allowing anterior migration in the absence of wounding. In our initial
331 establishment of our approach we chose to study two candidate molecules, *Smed-wnt1* (*wnt1*)
332 and *Smed-notum* (*notum*) that both seemed very likely candidates to be involved in both the
333 wound signal and anterior migration in the absence of wounding.

334 It has been previously shown that wounding at any sites results in the transcriptional
335 expression of *wnt1* in muscle cells at the wound site[36]. Given that Wnt signaling has a role in
336 regulating cell migration[37,38], we hypothesized that Wnt1 resulting from wound-induced
337 expression could be required for normal migration. We performed *wnt1(RNAi)* and observed
338 full penetrance of the tailless phenotype previously described for these animals
339 (Supplementary Figure 5A)[36]. However, in the context of our migration assay we observed no
340 effects on anterior migration after wounding suggesting *wnt1*, despite having wound induced
341 expression has no essential role in this process (Figure 7A-C and G-K).

342 *Smed-notum* is also expressed in muscle cells on wounding, but only at anterior facing
343 wounds where it is required to ensure the proper specification of anterior fates, probably by
344 repressing Wnt signaling[39]. Additionally it has a homeostatic expression pattern at the anterior
345 margin and has previously been shown to promote the homeostasis and correct size of the
346 brain in combination with the activity of a *wnt11-6* gene expressed in posterior brain
347 regions[29]. On this basis *notum* represents a candidate molecule for both wound induced
348 migration and migration of cells in anterior regions. We performed *notum(RNAi)* and
349 observed full penetrance of the double tailed phenotype previously described for these

350 animals in a standard regeneration assay (Supplementary Figure 5A)[39]. After shielded
351 irradiation and wounding we observed that animals recovered normally over a similar time
352 and we observed no difference in migration of cells or migrating cell morphology using
353 WFISH (Figure 7A-F, J and K). However, when using an anteriorly positioned shield, which
354 led to anterior migration of cells in control intact *GFP(RNAi)* animals, we observed a
355 significant reduction anterior migration in *notum(RNAi)* (Figure 7L-S). We note that this
356 reduction is not accompanied by a difference in the number of cells with cell extensions,
357 suggesting that notum may act by contributing a directional signal rather than one that
358 activates migratory behavior of anteriorly positioned stem cells and stem cell progeny. These
359 data suggest that *notum* is not essential for wound-induced cell migration but is required in the
360 case of anterior migration in intact animals that we uncovered in this work. It seems likely
361 that an the earlier description of a *notum/wnt11-6* regulatory circuit involved in homeostatic
362 regulation of brain size may also have a broader role in the homeostatic maintenance of
363 anterior regions that do not normally contain cycling stem cells.

364

365 **Discussion**

366 **An X-ray shielded assay allows precise observation of cell migration and application of**
367 **functional genomic approaches**

368 Here we have established a robust and reliable method that allows the regenerative planarian
369 model system to be used to study cell migration. During homeostasis as well as standard
370 regeneration experiments, stem cells and stem cell progeny are always close to where they are
371 required. Nonetheless, as with all metazoans reliant on adult stem cells, they must still move
372 short distances as they move and adjust into the correct functional positions in the tissues and
373 organs. In the case of very anterior region and the pharynx of the planarians body plan, that
374 are devoid of dividing stem cells, homeostasis must be achieved by migration of stem cell
375 progeny (Supplementary Figure 2A). However precise monitoring of this process is difficult
376 as the migratory distances involved are short and so confidently inferring changes in
377 migratory behavior as oppose to changes in, say, differentiation is not possible. Our X-ray
378 shielded assay creates a 'blank canvas' into which migrating stem cells and stem cell progeny
379 move and we can accurately assign relationships between migration, differentiation and
380 proliferation of groups of these cells over time. The innovations we have made here compared

381 to earlier approaches[7] allow for a thinner shield, smaller worms to be irradiated and technical
382 consistency over relatively large numbers of worms. This has allowed us to combine WFISH
383 and RNAi approaches so that we can now leverage the strength of the planarian model to
384 study cell migration. Combining these with assessment of gene expression in defined FACS
385 sorted cell populations will be make planarians a powerful model system for studying stem
386 cell migration in a regenerative context[40–42].

387 **A detailed description of migratory behavior in a regenerative context**

388 In this work we have revealed a number of detailed properties of cell migration in planarians
389 that can be used to help unpick the mechanisms controlling cell migration. We have shown
390 that migration occurs in response to wounding or damaged tissue as previously described[7], but
391 we find that posteriorly positioned stripes of stem cells do not migrate until tissue has
392 regressed towards them demonstrating damaged tissue only activates migration within a
393 certain range. We also find that contrary to previous work that migration can occur without
394 wounding or failure in tissue homeostasis for anteriorly positioned stem cells and stem cell
395 progeny. This observation tallies with the absence of stem cells in anterior regions and the
396 brain in intact animals, which means that a mechanism for encouraging significant
397 homeostatic cell migration must exist. We also observe that migrating cells home precisely to
398 wounds without initially recognizing other tissue regions lacking stem cells and stem cell
399 progeny. The observations dorsal *prog1*$^+$ cells migrate more rapidly than ventrally positioned
400 *prog1*$^+$ cells and that dorsal *smedwi-1*$^+$ cells migrate centrally along the midline and ventral
401 *smedwi-1*$^+$ cells in more lateral regions likely reflect the nature of underlying signaling
402 systems. Finally, improvements in in-situ hybridization methodology allow us to observe that
403 in regions containing moving cells we can see a clear increase in the number of cells with
404 pronounced cell extensions. Migrating cells are unconnected to other migrating cells, and
405 together these observations give an EMT like characteristic to planarians cell migration, as
406 oppose to other mechanism involving collective cell migration. Together these observations
407 establish a set of basic phenotypic criteria that can be used to the study the genetic control of
408 migration.

409 **The relationship between stem cell migration, proliferation and differentiation**

410 Stem cell migration during normal healthy tissue homeostasis must be intricately linked to
411 cell divisions, differentiation and integration of new cells to ensure dysfunctional aged and

412 damaged differentiated cells are successfully replaced. Studying this process *in vivo* during
413 adult tissue homeostasis has proven to be challenging and remains limited to a few contexts.
414 Clearly highly regenerative animal models represent an opportunity to study these processes,
415 which together power regeneration. Thus, perhaps the most important observations facilitated
416 by our assay are those concerning the relationships between migration, proliferation and
417 differentiation.

418 We observe that stem cell progeny migrate in large numbers in an initial response to
419 wounding and that proliferating stem cells accompany them in smaller numbers. In response
420 to both wounding and homeostatic signals we observe that stem cells divide asymmetrically
421 as they migrate, and that the divided progeny differentiate further while they migrate. This
422 creates an order of migration that recapitulates the known differentiation process for the
423 epidermal lineage (Figure 5L). We do not see any evidence that progeny slow down their
424 differentiation process in order to reach first wound sites and then differentiate. Instead our
425 observations broadly recapitulate cell behaviour observed during regeneration, in which
426 progeny migrate to form the regeneration blastema where they complete differentiation and
427 cycling cells follow later. Our analysis detects significant difference in migration between
428 *smedwi-1*$^{+}$ cells and zeta class/*smedwi-1*$^{-}$ cells, which we interpret as, suggesting that newly
429 minted progeny migrate ahead of cycling stem cells as they do in blastema formation. Stem
430 cells may migrate more slowly on average as they stop to divide, as they require the presence
431 of advanced progeny at certain density before they can be healthily maintained in a
432 repopulating tissue region or simply perhaps because they are slower due to having smaller
433 cell extensions. Based on these observations we note that our assay will provide an alternate
434 method of assessing cell lineage relationships with WFISH approaches and when combined
435 with RNAi it allows the molecular processes controlling the interplay between migration,
436 proliferation and differentiation to be studies. For example, future experiments can test the
437 requirement of migrating stem cells for stem cell progeny by interfering with differentiation
438 or asymmetric division.

439 Related to the observation that the order of cell migration we observe recapitulates cell
440 lineages is the question of whether all types of wound will result in the same or different
441 combinations of migratory, proliferative and differentiation responses. While we have
442 established that migration homes precisely to wound sites and we might expect differences in
443 proliferative response to relate to those already described for regeneration, we can also study

444 if differentiation programs show specificity to the type of wounds depending on which cell
445 types are damaged. Combining our assay with experimental paradigms that damage one or
446 few defined cell types, for example taking advantage accessibility of the photoreceptors or
447 drug targeting specific neuronal subsets, will help begin to answer how demands for new cells
448 is regulated and how stem cells and their progeny sense and adjust to these demands. Given
449 that these are likely to be the processes that decline in human age related disease or are mis-
450 regulated during tumour progression, planarian experiments in this context may provide
451 important new insights.

452 **Conservation of *Snail* function and the potential to study processes relevant to tumor**
453 **formation.**

454 The fact that cells appear to migrate individually and that in migratory regions increased
455 numbers of cells have extended cell processes as opposed to a rounded morphology suggested
456 molecular mechanisms associated with EMT may regulate migration. In order to begin to test
457 this possibility we investigated the function of a planarian *Snail* family transcription factor, as
458 this family is a key positive regulator cell migration during EMT, required to down regulate
459 the expression of genes that encode proteins that maintain cell-cell contacts like E-cadherin
460 and beta-integrins[31]. Enhanced *Snail* gene expression has reported in several different cancer
461 types including ovarian carcinoma[43], breast tumours[44,45]; gastric cancers[46,47]; hepatocellular
462 carcinomas[48,49]; colon cancers[50]; uterine cervix cancer[51] and synovial sarcomas[52].
463 Overexpression or down regulation of *Snail* has shown to modulate invasiveness and
464 metastasis in in vitro cancer cell culture studies[51,53–59]. These reports clearly suggest that *Snail*
465 is key player in cancer invasion and metastasis.

466 We found no phenotype for this gene using RNAi and in a standard amputation regeneration
467 assay; animals were able to regenerate normally. However, within the context of our assay
468 *snail(RNAi)* led to failure in cell migration compared to controls and we were able to clearly
469 observe decrease in cells showing extended cell processes, indicative of migratory
470 morphology. Our data confirm the role of a snail family gene in controlling migration in the
471 context for our assay and suggest we can use this as a basis for studying EMT related
472 processes in planarians. Given that the inappropriate activity of EMT underpins key parts of
473 cancer related pathology this will be an important future direction. By combining functional
474 approaches with expression screens starting with *snail*, other planarian homologs of EMT-
475 related transcription factor regulators and known upstream EMT regulatory signals, we will

476 be able to find out more about EMT in the context of tissue homeostasis and stem cell
477 activity.

478 **A role for *notum* in homeostatic migration of stem cells stem cell progeny.**

479 The precise identity of the signals that trigger migration after wounding remains an open
480 question. It seems more than likely that many overlapping signals cooperate to ensure
481 migration occurs correctly and it is likely to include signals associated primarily with
482 occurrence of damage as well as signals from specific tissues that require specific progeny.
483 Two genes that have already been shown to have complementary roles in controlling the
484 polarity of planarian regeneration, *wnt-1* and *notum*, are both known to be wound induced[39]
485 and represented good candidates for potential roles in cell migration after wounding. In
486 addition homeostatic expression of notum was recently shown to be involved in regulating
487 planarian brain size in combination with *wnt11-6*, and specifically ensuring that sufficient
488 neural precursors are produced to maintain the correct brain size[29]. These observations
489 therefore also make *notum* a candidate for involvement in the homeostatic cell migration that
490 we described in intact animals in anterior regions.

491 Using RNAi we found no role for either *wnt-1* or *notum* in wound induced migration,
492 however we found that *notum* required for the homeostatic anterior migration. Given the
493 homeostatic expression of *notum* transcript and the observation that cells migrate
494 homeostatically within a certain distance from the anterior tip of the animal, we propose that a
495 gradient of *notum* somehow provides directional cues to migrating cells. We note that, the
496 formation of cell extensions is not effected by *notum(RNAi)*, suggesting that other signals
497 maybe responsible for this aspect of migratory activity while *notum* provides a directional
498 cue. *notum* in planarians, mammals and flies has been implicated as a Wnt signaling
499 inhibitor[60–62], so it is possible that inhibition of local homeostatic levels of Wnt signaling,
500 specifically of anteriorly expressed planarian Wnts (*wnt11-6* and *wnt5*) may then allow
501 homeostatic migration. Future work with our assay will aim to understand the mechanism by
502 which *notum* facilitates homeostatic migration and it's relationship with wound induced
503 migration.

504 **Materials and methods**

505 **Planarian culture:**

506 A *Schmidtea mediterranea* asexual strain was cultured and maintained in 0.5% instant ocean
507 water in the dark at 20ºC. Animals were starved at least 7 days before using for experiments.

508 **X-ray irradiation, and design of shield**

509 Irradiations were performed using a Comet MXR-321 x-ray set operated at 225 kVp, 17mA
510 with a 0.5 mm aluminium filter. The X-ray field is collimated to 40 mm x 20 mm with a 6.1
511 mm thick lead disc positioned centrally, directly above the X-ray tube focal spot and
512 supported within an aluminium frame. The removable central shielded area is achieved using
513 a 0.8 mm wide, 6.1 mm thick lead strip spanning the long axis of the collimated field, this sits
514 slightly proud of the main lead collimator so that it is in contact with the base of the Petri
515 dish. When in position, the worms are irradiated at a dose rate of 23 Gy/min, reducing to ~ 1
516 Gy/min underneath the shielded region. The variation in dose distribution across the strip is
517 shown in supplementary figure 1C. The circular hole in the top aluminium plate corresponds
518 to the outside diameter of the Petri dish and enables dishes to be positioned quickly and
519 reproducibly. Thin strips of materials such as tungsten or tantalum could be used to replace
520 the lead strip to achieve thinner shielded regions if required.

521 **Dosimetry**

522 Dose rate measurements and spatial characterization of the treatment field was performed
523 using Gafchromic EBT3 film (International Specialty products, Wayne, NJ) placed in the base
524 of an empty 60 mm Petri dish. Twenty-four hours following exposure the EBT3 film was
525 scanned in transmission mode at 48 bit RGB (16 bits per colour) with 300 dpi resolution using
526 a flatbed scanner (Epson Expression 10000XL). A template was used to position the film
527 within the scanner and the scanning direction was kept constant with respect to the film
528 orientation, as recommended in the manufacturer's guidelines. The dose was calculated using
529 the optical density of the red channel and corrected using the optical density of the blue
530 channel in order to compensate for small non-uniformities in the film which cause false
531 apparent variations in dose (as described in the technical brief: *Gafchromic EBT2 Self-*
532 *developing film for radiotherapy dosimetry*). The batch of EBT3 film was calibrated
533 following the recommendations of the report of AAPM Task Group 61[63].

534 **Shielded irradiation:**

535 Up to 20 size-matched planarians (3 to 4 mm) were anesthetized in ice cold 0.2% chloretone
536 and aligned on 60mm Petri dish[64]. Anterior tip of all worms were aligned in a perfect line to
537 keep the absolute migratory distance (distance between tip of the head and shielded region)
538 fixed. Petri dish is pre-marked with a line at bottom denoting the place and dimensions (length
539 and thickness) of the shield strip. Excess liquid is removed to minimize movement of worms
540 during at the time of irradiation. Petri dish containing worms is then placed on to the shield of
541 bottom source X-ray irradiator. Care is taken to perfectly match the position of shield trip and
542 line marked on Petri dish to ascertain the exact region of the worm to be shielded. 30Gy X-ray
543 (225kV for 1 min 18 seconds) is used for irradiation. Once irradiation is over, planarians were
544 immediately washed with instant ocean water and transferred into fresh instant ocean water
545 and incubated in dark at 20ºC.

546 **WFISH, immunostaining and imaging**

547 Whole mount fluorescent in-situ hybridization was performed as described previously [65,66].
548 H3ser10p rabbit monoclonal antibody from Millipore (04–817) was used for immunostaining
549 [67]. Confocal imaging was done with Olympus FV1000 and Zeiss 880 Airyscan microscope.
550 Bright field images were taken with Zeiss Discovery V8 from Carl Zeiss using Canon 1200D
551 camera. Images were processed with Fiji and Adobe Photoshop. ZEN 2.1 (blue edition)
552 software from Carl Zeiss was used to construct 3D images of cells. All measurements and
553 quantifications were done with Fiji and Adobe Photoshop. Significance was determined by
554 unpaired 2-tailed Student's t-test.

555 **Gene cloning and RNAi**

556 Planarian genes were cloned into the pPR-T4P plasmid vector containing opposable T7 RNA
557 polymerase promoters (kind gift from Jochen Rink). The cloned vectors were then used for in
558 vitro dsRNA synthesis and probe synthesis as described previously [65,68]. Previously described
559 sequence regions were used for dsRNA synthesis of *MMPa*[30], *Wnt1*[36] and *Notum*[39]. *Snail*
560 dsRNA was synthesized by using forward primer GTTATCAAGCCAGACCTTCA and
561 reverse primer GTTTGACTTGTGAATGGGTC. Reported sequences were used for riboprobe
562 synthesis of *smedwi-1*[69], *prog-1*[18], *agat-1*[18], zeta pool[4], and sigma pool[4]. For knockdown of
563 genes animals were injected with 3 x 32nl of dsRNA 6 times over 2 weeks. If worms need to
564 be used for shielded irradiation after RNAi, a 1-day gap was kept between last RNAi injection
565 and the shielded irradiation.

Acknowledgments

We thank all members of the Aboobaker lab past and present for discussions and reagent sharing.

Funding

The work of PA, EA, NK, AAA is funded by the MRC (grant number MR/M000133/1), BBSRC (grant number BB/K007564/1), the John Fell Fund Oxford University Press (OUP), and a small grant from the CRUK Oxford Centre. NK is funded by a Marie Curie Sklodowska fellowship funded by Horizon 2020. MH and JT acknowledge funding from the Funding from Medical Research Council Strategic Partnership Funding (MC-PC-12004) for the CRUK/MRC Oxford Institute for Radiation Oncology is gratefully acknowledged.

References

1. Gehrke, A. R. & Srivastava, M. Neoblasts and the evolution of whole-body regeneration. *Curr. Opin. Genet. Dev.* **40,** 131–137 (2016).
2. Tanaka, E. M. Regeneration: if they can do it, why can't we? *Cell* **113,** 559–62 (2003).
3. Wagner, D. E., Wang, I. E. & Reddien, P. W. Clonogenic neoblasts are pluripotent adult stem cells that underlie planarian regeneration. *Science* **332,** 811–6 (2011).
4. van Wolfswinkel, J. C., Wagner, D. E. & Reddien, P. W. Single-Cell Analysis Reveals Functionally Distinct Classes within the Planarian Stem Cell Compartment. *Cell Stem Cell* **15,** 326–339 (2014).
5. Reig, G., Pulgar, E. & Concha, M. L. Cell migration: from tissue culture to embryos. *Development* **141,** 1999–2013 (2014).
6. Bradshaw, B., Thompson, K. & Frank, U. Distinct mechanisms underlie oral vs aboral regeneration in the cnidarian Hydractinia echinata. *Elife* **4,** (2015).
7. Guedelhoefer, O. C. & Sánchez Alvarado, A. Amputation induces stem cell mobilization to sites of injury during planarian regeneration. *Development* **139,** 3510–20 (2012).

595 8. Friedl, P. & Gilmour, D. Collective cell migration in morphogenesis, regeneration and
596 cancer. *Nat. Rev. Mol. Cell Biol.* **10,** 445–57 (2009).
597 9. Feng, L., Wei, W., Heng, Z., Yantao, H. & Chunbo, W. Knockdown of REV7 Inhibits
598 Breast Cancer Cell Migration and Invasion. *Oncol. Res.* **24,** 315–325 (2016).
599 10. Goichberg, P. Current Understanding of the Pathways Involved in Adult Stem and
600 Progenitor Cell Migration for Tissue Homeostasis and Repair. *Stem Cell Rev.* **12,** 421–
601 37 (2016).
602 11. Friedl, P., Locker, J., Sahai, E. & Segall, J. E. Classifying collective cancer cell
603 invasion. *Nat. Cell Biol.* **14,** 777–83 (2012).
604 12. Friedl, P. & Alexander, S. Cancer invasion and the microenvironment: plasticity and
605 reciprocity. *Cell* **147,** 992–1009 (2011).
606 13. Ridley, A. J. *et al.* Cell migration: integrating signals from front to back. *Science* **302,**
607 1704–9 (2003).
608 14. Montell, D. J. Border-cell migration: the race is on. *Nat. Rev. Mol. Cell Biol.* **4,** 13–24
609 (2003).
610 15. Geisbrecht, E. R. & Montell, D. J. Myosin VI is required for E-cadherin-mediated
611 border cell migration. *Nat. Cell Biol.* **4,** 616–20 (2002).
612 16. Sato, K. *et al.* Left-right asymmetric cell intercalation drives directional collective cell
613 movement in epithelial morphogenesis. *Nat. Commun.* **6,** 10074 (2015).
614 17. Hagedorn, E. J. *et al.* The netrin receptor DCC focuses invadopodia-driven basement
615 membrane transmigration in vivo. *J. Cell Biol.* **201,** 903–13 (2013).
616 18. Eisenhoffer, G. T., Kang, H. & Sánchez Alvarado, A. Molecular analysis of stem cells
617 and their descendants during cell turnover and regeneration in the planarian Schmidtea
618 mediterranea. *Cell Stem Cell* **3,** 327–39 (2008).
619 19. Aboobaker, a A. Planarian stem cells: a simple paradigm for regeneration. *Trends Cell*
620 *Biol.* **21,** 304–11 (2011).
621 20. Forsthoefel, D. J. & Newmark, P. a. Emerging patterns in planarian regeneration. *Curr.*
622 *Opin. Genet. Dev.* **19,** 412–20 (2009).
623 21. Rink, J. C., Gurley, K. a, Elliott, S. a & Sánchez Alvarado, A. Planarian Hh signaling
624 regulates regeneration polarity and links Hh pathway evolution to cilia. *Science* **326,**
625 1406–10 (2009).
626 22. Reddien, P. W., Bermange, A. L., Kicza, A. M. & Sánchez Alvarado, A. BMP
627 signaling regulates the dorsal planarian midline and is needed for asymmetric
628 regeneration. *Development* **134,** 4043–51 (2007).

629 23. Wurtzel, O. *et al*. A Generic and Cell-Type-Specific Wound Response Precedes
630 Regeneration in Planarians. *Dev. Cell* **35,** 632–45 (2015).
631 25. Wolff, E. Recent researches on the regeneration of planaria. in *'Regeneration. 20th*
632 *Growth Symposium' (D. Rudnick, Ed)* 53–84 (Ronald Press, 1962).
633 26. Dubois, F. Contribution á l 'ètude de la migration des cellules de règènèration chez les
634 Planaires dulcicoles. *Bull. Biol. Fr. Belg.* **83,** 213–283 (1949).
635 27. Tasaki, J., Uchiyama-Tasaki, C. & Rouhana, L. Analysis of Stem Cell Motility In Vivo
636 Based on Immunodetection of Planarian Neoblasts and Tracing of BrdU-Labeled Cells
637 After Partial Irradiation. *Methods Mol. Biol.* **1365,** 323–38 (2016).
638 28. Pearson, B. J. *et al*. Formaldehyde-based whole-mount in situ hybridization method for
639 planarians. *Dev. Dyn.* **238,** 443–50 (2009).
640 29. Hill, E. M. & Petersen, C. P. Wnt/Notum spatial feedback inhibition controls neoblast
641 differentiation to regulate reversible growth of the planarian brain. *Development*
642 (2015). doi:10.1242/dev.123612
643 30. Isolani, M. E. *et al*. Planarians as a Model to Assess In Vivo the Role of Matrix
644 Metalloproteinase Genes during Homeostasis and Regeneration. *PLoS One* **8,** (2013).
645 31. Thiery, J. P. & Sleeman, J. P. Complex networks orchestrate epithelial-mesenchymal
646 transitions. *Nat. Rev. Mol. Cell Biol.* **7,** 131–42 (2006).
647 32. Colvin Wanshura, L. E., Galvin, K. E., Ye, H., Fernandez-Zapico, M. E. & Wetmore,
648 C. Sequential activation of Snail1 and N-Myc modulates sonic hedgehog-induced
649 transformation of neural cells. *Cancer Res.* **71,** 5336–45 (2011).
650 33. Batlle, E. *et al*. The transcription factor snail is a repressor of E-cadherin gene
651 expression in epithelial tumour cells. *Nat. Cell Biol.* **2,** 84–9 (2000).
652 34. Cano, a *et al*. The transcription factor snail controls epithelial-mesenchymal transitions
653 by repressing E-cadherin expression. *Nat. Cell Biol.* **2,** 76–83 (2000).
654 35. Scimone, M. L., Kravarik, K. M., Lapan, S. W. & Reddien, P. W. Neoblast
655 Specialization in Regeneration of the Planarian Schmidtea mediterranea. *Stem cell*
656 *reports* **3,** 339–352 (2014).
657 36. Petersen, C. P. & Reddien, P. W. A wound-induced Wnt expression program controls
658 planarian regeneration polarity. *Proc. Natl. Acad. Sci. U. S. A.* **106,** 17061–6 (2009).
659 37. Vlad-Fiegen, A., Langerak, A., Eberth, S. & Müller, O. The Wnt pathway destabilizes
660 adherens junctions and promotes cell migration via β-catenin and its target gene cyclin
661 D1. *FEBS Open Bio* **2,** 26–31 (2012).
662 38. Aman, A. & Piotrowski, T. Wnt/beta-catenin and Fgf signaling control collective cell

663 migration by restricting chemokine receptor expression. *Dev. Cell* **15,** 749–61 (2008).
664 39. Petersen, C. P. & Reddien, P. W. Polarized notum activation at wounds inhibits Wnt
665 function to promote planarian head regeneration. *Science* **332,** 852–5 (2011).
666 40. Romero, B. T., Evans, D. J. & Aboobaker, A. A. in (eds. Mace, K. A. & Braun, K. M.)
667 **916,** 167–179 (Humana Press, 2012).
668 41. Hayashi, T. & Agata, K. A unique FACS method to isolate stem cells in planarian.
669 *Methods Mol. Biol.* **879,** 29–37 (2012).
670 42. Solana, J. *et al.* Defining the molecular profile of planarian pluripotent stem cells using
671 a combinatorial RNAseq, RNA interference and irradiation approach. *Genome Biol.* **13,**
672 R19 (2012).
673 43. Davidson, B., Tropé, C. G. & Reich, R. Epithelial-mesenchymal transition in ovarian
674 carcinoma. *Front. Oncol.* **2,** 33 (2012).
675 44. Blanco, M. J. *et al.* Correlation of Snail expression with histological grade and lymph
676 node status in breast carcinomas. *Oncogene* **21,** 3241–6 (2002).
677 45. Elloul, S. *et al.* Snail, Slug, and Smad-interacting protein 1 as novel parameters of
678 disease aggressiveness in metastatic ovarian and breast carcinoma. *Cancer* **103,** 1631–
679 43 (2005).
680 46. Peng, Z., Wang, C.-X., Fang, E.-H., Wang, G.-B. & Tong, Q. Role of epithelial-
681 mesenchymal transition in gastric cancer initiation and progression. *World J.*
682 *Gastroenterol.* **20,** 5403–10 (2014).
683 47. Rosivatz, E. *et al.* Differential expression of the epithelial-mesenchymal transition
684 regulators snail, SIP1, and twist in gastric cancer. *Am. J. Pathol.* **161,** 1881–91 (2002).
685 48. Miyoshi, A. *et al.* Snail accelerates cancer invasion by upregulating MMP expression
686 and is associated with poor prognosis of hepatocellular carcinoma. *Br. J. Cancer* **92,**
687 252–8 (2005).
688 49. Sugimachi, K. *et al.* Transcriptional repressor snail and progression of human
689 hepatocellular carcinoma. *Clin. Cancer Res.* **9,** 2657–64 (2003).
690 50. Pálmer, H. G. *et al.* The transcription factor SNAIL represses vitamin D receptor
691 expression and responsiveness in human colon cancer. *Nat. Med.* **10,** 917–9 (2004).
692 51. Myong, N.-H. Loss of E-cadherin and Acquisition of Vimentin in Epithelial-
693 Mesenchymal Transition are Noble Indicators of Uterine Cervix Cancer Progression.
694 *Korean J. Pathol.* **46,** 341–8 (2012).
695 52. Saito, T. *et al.* E-cadherin mutation and Snail overexpression as alternative mechanisms
696 of E-cadherin inactivation in synovial sarcoma. *Oncogene* **23,** 8629–38 (2004).

697 53. Horvay, K. *et al*. Snai1 regulates cell lineage allocation and stem cell maintenance in
698 the mouse intestinal epithelium. *EMBO J*. **34,** 1319–35 (2015).
699 54. Adhikary, A. *et al*. Inhibition of epithelial to mesenchymal transition by E-cadherin up-
700 regulation via repression of slug transcription and inhibition of E-cadherin degradation:
701 dual role of scaffold/matrix attachment region-binding protein 1 (SMAR1) in breast
702 cancer cells. *J. Biol. Chem*. **289,** 25431–44 (2014).
703 55. Smith, B. N. *et al*. Snail promotes epithelial mesenchymal transition in breast cancer
704 cells in part via activation of nuclear ERK2. *PLoS One* **9,** e104987 (2014).
705 56. Sharili, A.-S., Allen, S., Smith, K., Price, J. & McGonnell, I. M. Snail2 promotes
706 osteosarcoma cell motility through remodelling of the actin cytoskeleton and regulates
707 tumor development. *Cancer Lett*. **333,** 170–9 (2013).
708 57. Villarejo, A. *et al*. Loss of Snail2 favors skin tumor progression by promoting the
709 recruitment of myeloid progenitors. *Carcinogenesis* **36,** 585–97 (2015).
710 58. Fan, F. *et al*. Overexpression of snail induces epithelial-mesenchymal transition and a
711 cancer stem cell-like phenotype in human colorectal cancer cells. *Cancer Med*. **1,** 5–16
712 (2012).
713 59. Belgiovine, C. *et al*. Snail levels control the migration mechanism of mesenchymal
714 tumor cells. *Oncol. Lett*. **12,** 767–771 (2016).
715 60. Zhang, X. *et al*. Notum is required for neural and head induction via Wnt deacylation,
716 oxidation, and inactivation. *Dev. Cell* **32,** 719–30 (2015).
717 61. Kakugawa, S. *et al*. Notum deacylates Wnt proteins to suppress signalling activity.
718 *Nature* **519,** 187–92 (2015).
719 62. Traister, A., Shi, W. & Filmus, J. Mammalian Notum induces the release of glypicans
720 and other GPI-anchored proteins from the cell surface. *Biochem. J*. **410,** 503–11
721 (2008).
722 63. Ma, C. M. *et al*. AAPM protocol for 40-300 kV x-ray beam dosimetry in radiotherapy
723 and radiobiology. *Med. Phys*. **28,** 868–93 (2001).
724 64. Guedelhoefer, O. C. & Sánchez Alvarado, A. Planarian immobilization, partial
725 irradiation, and tissue transplantation. *J. Vis. Exp*. 1–7 (2012). doi:10.3791/4015
726 65. King, R. S. & Newmark, P. a. In situ hybridization protocol for enhanced detection of
727 gene expression in the planarian Schmidtea mediterranea. *BMC Dev. Biol*. **13,** 8 (2013).
728 66. Currie, K. W. *et al*. HOX gene complement and expression in the planarian Schmidtea
729 mediterranea. *Evodevo* **7,** 7 (2016).
730 67. Felix, D. a & Aboobaker, a A. The TALE class homeobox gene Smed-prep defines the

731 anterior compartment for head regeneration. *PLoS Genet*. **6,** e1000915 (2010).
732 68. Rouhana, L. *et al*. RNA interference by feeding in vitro-synthesized double-stranded
733 RNA to planarians: methodology and dynamics. *Dev. Dyn*. **242,** 718–30 (2013).
734 69. Reddien, P. W., Oviedo, N. J., Jennings, J. R., Jenkin, J. C. & Sánchez Alvarado, A.
735 SMEDWI-2 is a PIWI-like protein that regulates planarian stem cells. *Science* **310,**
736 1327–30 (2005).
737
738
739 **Figure Legends**
740
741 **Figure 1. Shielded irradiation assay setup:**
742 (A) Point source X-ray irradiator with the lead shield on top and holding worms aligned in a
743 Petri dish.
744 (B) Worms anesthetized in 0.2% chloretone and aligned in a straight line on 60mm Petri dish.
745 (C) Lead shield with a horizontal lead stripe in the middle.
746 (D-E) Wild type un-irradiated planarians showing distribution of stem cells (green) and early
747 progeny (magenta) (D). Striped planarians at 4 days post shielded irradiation (4dpi) showing
748 band of stem cells (green) and early progeny (magenta) restricted in irradiation-protected
749 region (E). 30 Gy X-ray is used.
750 (F) Gradual loss of stem cells (green) and early progeny (magenta) from non-shielded region
751 after 1 dpi, 2dpi, 3dpi and 4dpi respectively (n=10).
752
753 **Supplementary Figure 1. Parts and dimensions of lead shield assembly:**
754 (A) Lead strip and lead shield are assembled with aluminium support which further covered
755 with aluminium disc to support Petri dish in the final lead shield assembly.
756 (B) Dimensions of lead shield and lead strip from top and side view. Unit: mm.
757 (C) Dose distribution across the lead strip showing greater than 94% attenuation of X-ray dose
758 under the lead strip protected region.
759
760 **Figure 2. Anterior migration and repopulation of stem cells and stem cell progeny in**
761 **uninjured animals:**
762 (A) Cartoon showing strategy of shielding worms at various places along the anterior-
763 posterior axis.

764 (B-J) Bright field images of worms shielded at 3 different places posterior (B, C), middle (E,
765 F) and anterior (H, I) in shielded irradiation assay showing regression and recovery over the
766 time. Bright field images show head regression in posteriorly shielded worms (B), head and
767 tail regression in middle shielded worms (E) and tail regression in anteriorly shielded worm
768 (H). As cells migrate and repopulate the regressed anterior and posterior regions recovered
769 over the time in all posterior (C), middle (F) and anterior (I) shielded worms (n=20 per time
770 point). Scale bars: 500μm.
771 (D, G, J) FISH showing no migration of stem cells (green) and early progeny (magenta) in
772 posteriorly shielded worms (D) until anterior tissue regress close enough to the shielded
773 region. Whereas stem cells (green) and early progeny (magenta) migrate and repopulate in the
774 anterior direction in some middle (G) and anteriorly (J) shielded worms (n=20 per time point).
775 Migration takes less time in anteriorly placed shields. Scale bars: 500μm.
776 (K) Measurements of distance migrated by stem cells (green) and early progeny (magenta) in
777 the worms shielded irradiated at different places along AP axis. Each dot represent distance
778 migrated by individual cell in each animal. Distance of 10 most distal cells of each class is
779 measured from each animal (n=16).
780 (L) Model showing gradient of signal (orange) form head tip to up to ~1300μm towards
781 posterior.
782
783 **Supplementary Figure 2. Distribution of stem cells in intact and regenerating animals:**
784 (A) FISH showing distribution of stem cells (green) in intact wild type worm. Stem cells are
785 absent in the pharynx region, in brain region and region anterior to photoreceptors (*). Scale
786 bar: 500μm.
787 (B) FISH showing that stem cells (green) are absent in the early regenerative blastema in a tail
788 fragment regenerating at 3dpa (n=5 per time point). Scale bar: 200μm.
789
790 **Figure 3. Migration and repopulation of stem cells and stem cell progeny in decapitated**
791 **animals:**
792 (A) Model demonstrating three different ways to measure distance of migrating cell. I)
793 Distance migrated by cell = distance between anterior boundary of the shielded region and
794 migrating cell (*X*), II) Distance migrated by cell = distance between posterior boundary of the
795 shielded region and migrating cell (*X*) – 0.8mm (length of the shielded region), III) Distance
796 migrated by cell = distance between posterior boundary of shielded region and anterior tip (*Y*)
797 – distance between anterior tip and migrating cell (*X*) – 0.8mm (length of the shielded region).

798 (B) FISH showing migration and repopulation of stem cells (green) and early progeny
799 (magenta) at 1, 4, 7 and 10 days post decapitation (n=10 per time point). Scale bars: 500μm.
800 (C) Measurements of distance migrated by stem cells (green) and early progeny (magenta) at
801 1, 4, 7 and 10 days post decapitation. Each dot represent average distance migrated by 10
802 most distal cells in each animal (n=25 per time point). Lines and error bars indicate mean and
803 SD.
804 (D) Stem cell to early progeny ratio in the migratory region is plotted at 1, 4, 7 and 10 days
805 post decapitation (n=10 per time point). Ratio of cells in shielded region and in unexposed
806 worm is used as control. The results are expressed as means ±SD.
807 (E) Quantification of stem cells (magenta) and mitotic cells (green) in the migratory region
808 following decapitation at 1, 4, 7 and 10 days (n=10 per time point). The results are expressed
809 as means ±SD.
810
811 **Supplementary Figure 3. Mitotic activity and other general features of cell migration in**
812 **planarians:**
813 (A) H3P immunostaining shows increase in mitotic cells (yellow) in the migratory region over
814 the time course, 1dpa, 4dpa, 7dpa and 10dpa (n=5 per time point). Scale bar: 500μm.
815 (B) Graph showing increasing distance of mitotic cells (magenta dots) from the shielded
816 region over the time course, 1dpa, 4dpa, 7dpa and 10dpa (n=5 per time point). Each dot
817 represents the distance of individual H3P cell from the shielded region. 5 most distal H3P
818 cells were considered for measurements from each animal. Lines and error bars indicate mean
819 and SD.
820 (C, D) Stem cells (green) and early progeny (magenta) show directional migration towards the
821 site of poking (C) and notch (D).
822 (E) Stem cells (green) and early progeny (magenta) from the dorsal side migrate more rapidly
823 than the ventral side. Scale bar: 100μm.
824 (F) Measurements of distance migrated by stem cells (green) and early progeny (magenta)
825 from dorsal and ventral side. Each dot represents average the distance migrated by 10 most
826 distal cells in an animal (n=5). Lines and error bars indicate mean and SD.
827 (G) Montage showing migrating stem cells (green) in different planes from dorsal to ventral
828 side.
829
830 **Figure 4. Stem cells and early progeny show extended cytoplasmic projections during**
831 **migration:**

832 (A) Morphology of cells within the shielded region in an uninjured worm shows very few
833 stem cells (green) and few early progeny cells (magenta) with extended cytoplasmic
834 projections (n=10).
835 (B) Morphology of cells within the shielded region in the decapitated worm shows few stem
836 cells (green) and some early progeny cells (magenta) with extended cytoplasmic projections
837 (n=10).
838 (C) Morphology of cells within the migratory region in the decapitated worm shows few stem
839 cells (green) and many early progeny cells (magenta) with extended cytoplasmic projections
840 (n=10).
841 (D) Quantification shows increase in number of stem cells (green) and early progeny cells
842 (magenta) with extended processes within decapitated/migratory region as well as
843 decapitated/shielded region compared to the uninjured/shielded region (n=10 per condition).
844 The results are expressed as means ±SD. Student's t test: *$p<0.05$.
845 (E-H) Early progeny cells (magenta) within migratory region in decapitated worms shows
846 extended processes in various directions. Yellow arrows indicate the direction of extended
847 processes.
848
849 **Supplementary Figure 4. Different shapes of cells:**
850 (A-B) Morphology of stem cells (green) and early progeny (magenta) without and with
851 extended processes.
852
853 **Figure 5. Migration of different epidermal lineage cells shows that cells migrate in the**
854 **specific order with most differentiated cells leading to the least differentiated cells:**
855 (A-J) FISH showing migration of different cell types in epidermal lineage at 7dpa. *Agat-1*
856 cells (magenta) migrate way ahead of *smedwi-1* cells (green) (A, B). *prog-1* cells (magenta)
857 migrate way ahead of *smedwi-1* cells (green) (C, D). *prog-1* cells (magenta), Zeta class cells
858 (green) and *prog-1* + Zeta class double positive cells (white) migrate with the similar speed
859 (E, F). smedwi-1 negative zeta class cells (magenta) migrate way ahead of *smedwi-1* positive
860 zeta stem cells (white) and *smedwi-1* cells (green) (G, H). *smedwi-1* positive sigma stem cells
861 (white) and *smedwi-1* cells (green) migrate with the similar speed (I, J) (n=5 per condition).
862 White arrows indicate the examples of double positive cells. Scale bars: 300μm for zoomed
863 out and 100μm for zoomed in view.
864 (K) Measurements of distance travelled by different cell populations (*smedwi-1* postive sigma
865 class stem cells, *smedwi-1* positive zeta class stem cells, *smedwi-1* negative zeta class cells,

866 *prog-1* + zeta class double positive cells, *prog-1* cells and *agat-1* cells) in decapitated worms
867 at 7dpa. (n=5 per condition, Student's t test: *p<0.05)
868 (L) Model demonstrating order in which different cells migrate following decapitation. *Agat-*
869 *1*, *prog-1*, *prog-1* + zeta class double positive cells migrate most anteriorly and are most distal
870 to the shielded region. Zeta class (*smedwi-1*$^{-}$) cells migrate equally with *prog-1*, *prog-1* + zeta
871 class double positive cells but are quite distant to *agat-1* cells. Zeta stem cells and sigma stem
872 cells migrate with the slowest speed and are most proximal to the shielded region.
873
874 **Figure 6. *MMPa*, *Snail* RNAi inhibit cell migration:**
875 (A-I) FISH shows migration of stem cells (green) and early progeny (magenta) at 7dpa in
876 GFP RNAi (A-C) worms but the migration is inhibited in *MMPa(RNAi)* (D-F) and reduced in
877 *SNAIL(RNAi)* (G-I) worms. Insets show the presence of stem cells (green) and early progeny
878 (magenta) with extended cytoplasmic projections in migratory region of *GFP(RNAi)* worms
879 (B, C) but are almost absent in *MMPa(RNAi)* (E, F) and *SNAIL(RNAi)* (H, I) worms (n=5).
880 (J) Measurements of shows drastic decrease in the distance migrated by stem cells (green) and
881 early progeny (magenta) at 7dpa in *MMPa(RNAi)* and *SNAIL(RNAi)* animals compared to
882 *GFP(RNAi)* worms (n=5). Each dot represents the average distance migrated by 10 most
883 distal cells from each animal. Lines and error bars indicate mean and SD. Student's t test:
884 *p<0.05.
885 (K) Quantification shows that stem cells (green) and early progeny (magenta) with extended
886 processes are reduced significantly in *MMPa(RNAi)* and *SNAIL(RNAi)* animals in comparison
887 with *GFP(RNAi)* animals at 7dpa (n=5). The results are expressed as means ±SD. Student's t
888 test: *p<0.05.
889 (L) Quantification shows reduction in stem cell to early progeny ratio in *SNAIL(RNAi)*
890 animals compared to *GFP(RNAi)* animals at 7dpa (n=5). Each dot represents the data from
891 individual animal. Lines and error bars indicate mean and SD. Student's t test: *p<0.05.
892
893 **Supplementary Figure 5. Bright field images showing penetrance of RNAi and its effect**
894 **on regeneration:**
895 (A) Head, Trunk and Tail fragments regenerated at 11 days post amputation following
896 *GFP(RNAi)*, *MMPa(RNAi)*, *SNAIL(RNAi)*, *Wnt1(RNAi)* and *Notum(RNAi)*. (n=10)
897 (B) Rescue and regeneration of *GFP(RNAi)*, *MMPa(RNAi)* and *SNAIL(RNAi)* worms
898 following shielded irradiation and decapitation. (n=30)
899

Figure 7. Effect of Notum RNAi and Wnt1 RNAi on cell migration:

(A-I) FISH showing migration of stem cells (green) and early progeny (magenta) at 7 days post decapitation in *GFP(RNAi)* (A-C) animals and is unaffected in *Notum(RNAi)* (D-F) and *Wnt-1(RNAi)* (G-I) animals. Insets show morphology of stem cells (green) and early progeny (magenta) in migratory region (B, C, E, F, H, I).

(J) Measurements show that distance migrated by stem cells (green) and early progeny (magenta) at 7 dpa in *GFP(RNAi)*, *Notum(RNAi)* and *Wnt-1(RNAi)* animals is similar (n=10). Each dot represents the average distance migrated by 10 most distal cells from each animal. Lines and error bars indicate mean and SD. Student's t test used for analysis.

(K) Quantification shows that the number of stem cells (green) and early progeny (magenta) with extended processes is unaffected in *Notum(RNAi)* and *Wnt-1(RNAi)* animals compared to *GFP(RNAi)* animals (n=10). The results are expressed as means ±SD. Student's t test used for analysis.

(L-Q) FISH showing reduced migration of stem cells (green) and early progeny (magenta) at 10dpi in intact *Notum(RNAi)* (O-Q) animals compared to intact *GFP(RNAi)* (L-N) animals. Insets show morphology of stem cells (green) and early progeny (magenta) in migratory region (M, N, P, Q).

(R) Measurements show that distance migrated by stem cells (green) and early progeny (magenta) at 10dpi in *Notum(RNAi)* animals is significantly reduced compared to *GFP(RNAi)* animals (n=10). Each dot represents the average distance migrated by 10 most distal cells from each animal. Lines and error bars indicate mean and SD. Student's t test: *$p<0.05$.

(S) Quantification shows that the number of stem cells (green) and early progeny (magenta) with extended processes is unaffected in *Notum(RNAi)* compared to *GFP(RNAi)* animals (n=10). The results are expressed as means ±SD. Student's t test used for analysis.

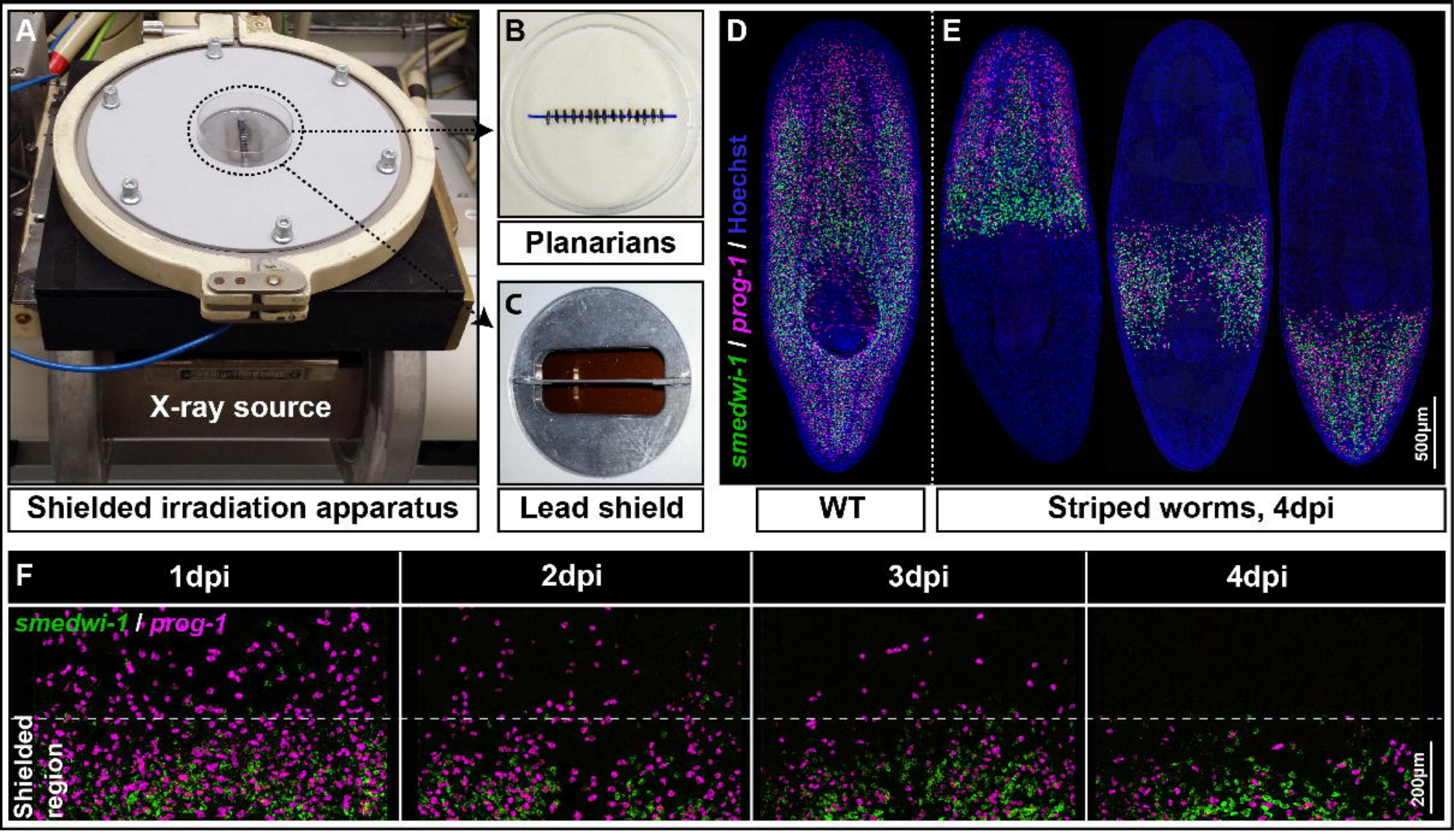
A
X-ray source
Shielded irradiation apparatus
B
Planarians
C
Lead shield
D
E
smedwi-1 / prog-1 / Hoechst
500µm
WT
Striped worms, 4dpi
F
1dpi
2dpi
3dpi
4dpi
smedwi-1 / prog-1
Shielded region
200µm

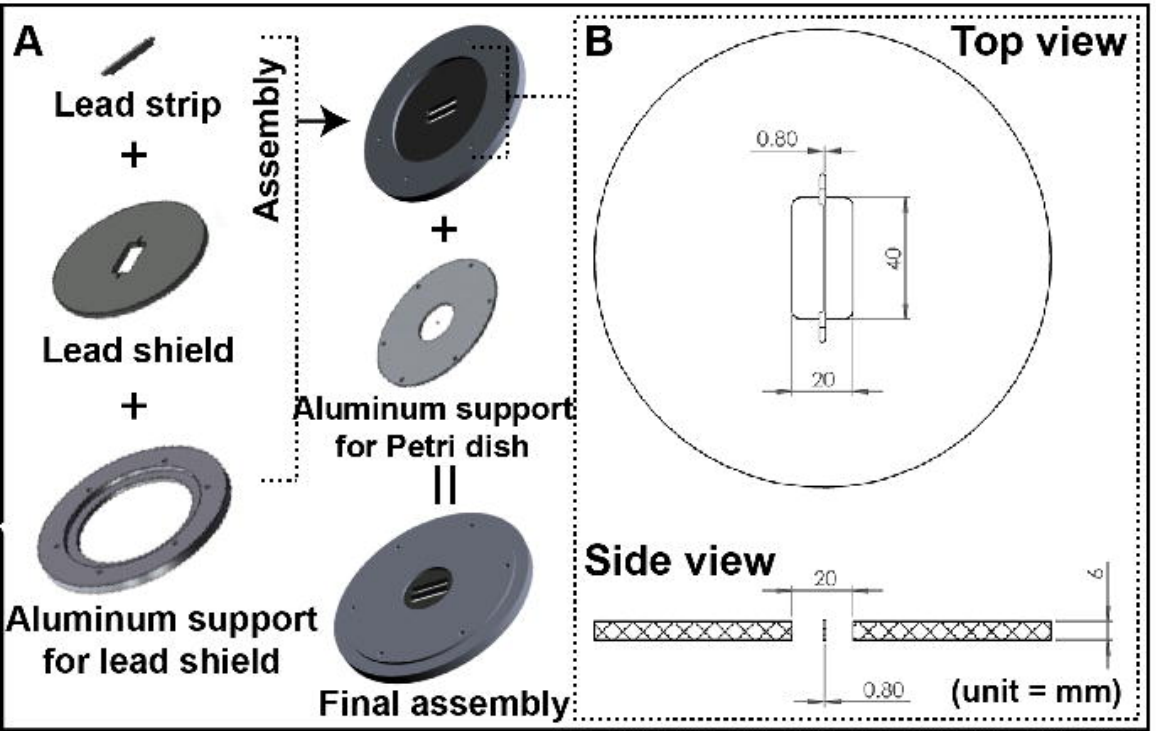
A
Lead strip
+
Lead shield
+
Aluminum support
for lead shield
Assembly
+
Aluminum support
for Petri dish
||
Final assembly
B
Top view
0.80
40
20
Side view
20
6
0.80
(unit = mm)

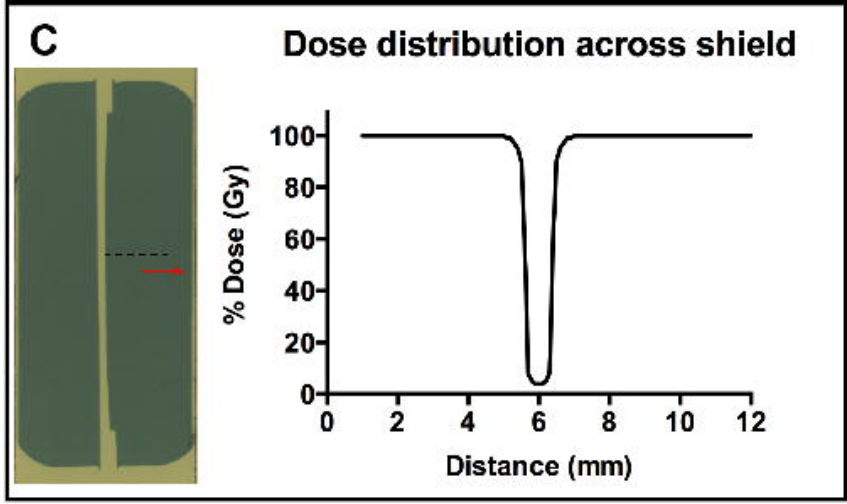
C
Dose distribution across shield
% Dose (Gy)
100
80
60
40
20
0
0
2
4
6
8
10
12
Distance (mm)

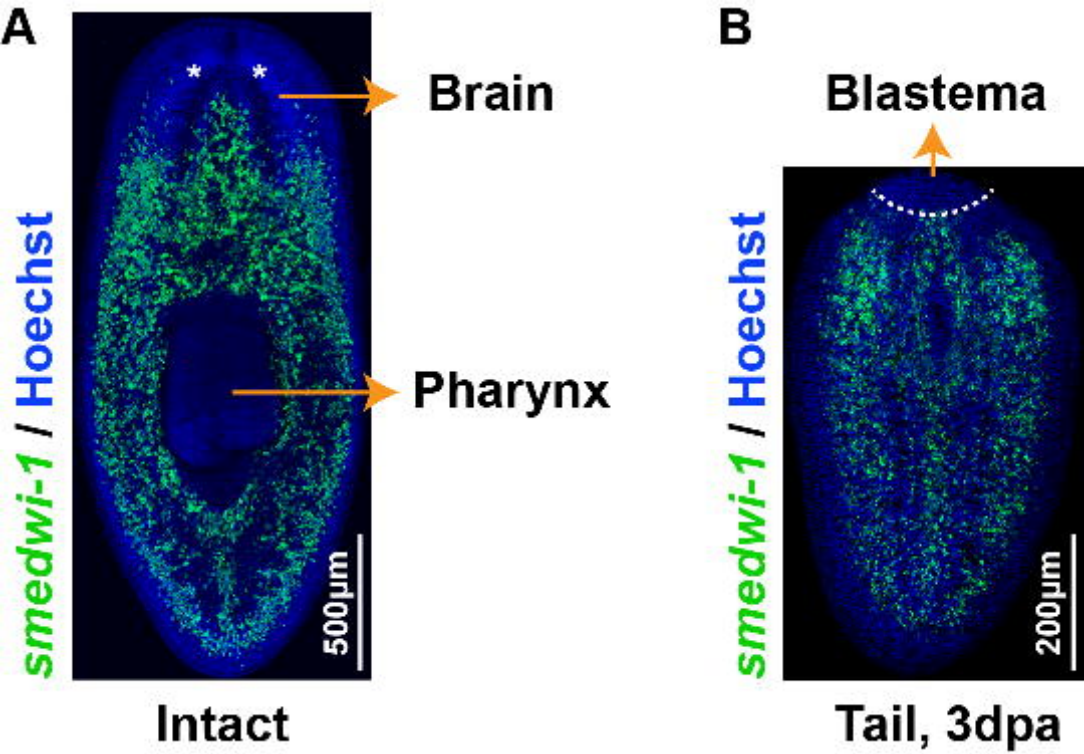
A
Brain
Pharynx
smedwi-1 / Hoechst
500µm
Intact
B
Blastema
smedwi-1 / Hoechst
200µm
Tail, 3dpa

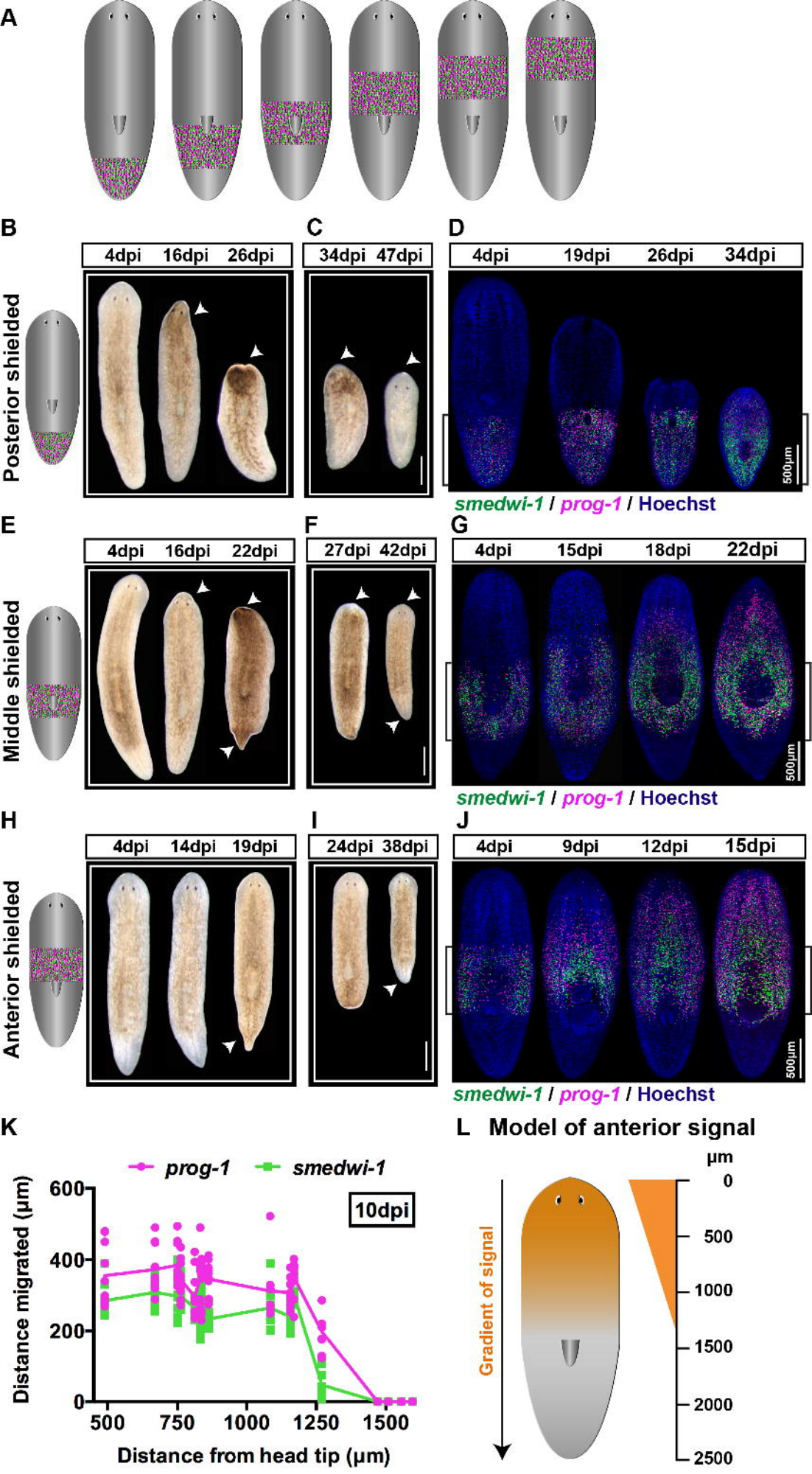
A
B
C
D
Posterior shielded
4dpi 16dpi 26dpi
34dpi 47dpi
4dpi 19dpi 26dpi 34dpi
500µm
smedwi-1 / prog-1 / Hoechst
E
F
G
Middle shielded
4dpi 16dpi 22dpi
27dpi 42dpi
4dpi 15dpi 18dpi 22dpi
500µm
smedwi-1 / prog-1 / Hoechst
H
I
J
Anterior shielded
4dpi 14dpi 19dpi
24dpi 38dpi
4dpi 9dpi 12dpi 15dpi
500µm
smedwi-1 / prog-1 / Hoechst
K
prog-1
smedwi-1
10dpi
Distance migrated (µm)
600
400
200
0
500 750 1000 1250 1500
Distance from head tip (µm)
L Model of anterior signal
µm
0
500
1000
1500
2000
2500
Gradient of signal

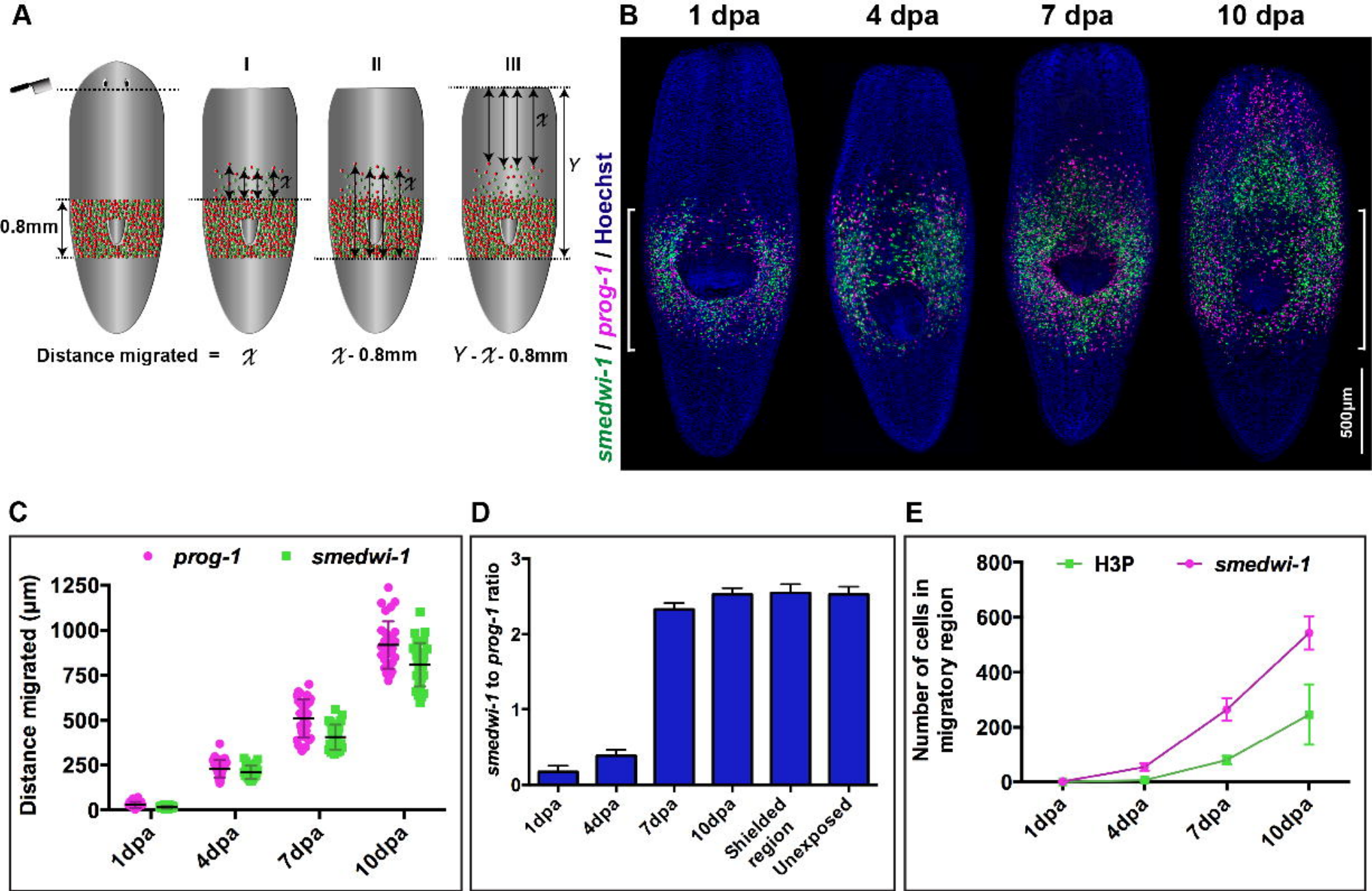
A
I
II
III
0.8mm
Distance migrated = x
x - 0.8mm
Y - x - 0.8mm
B
1 dpa
4 dpa
7 dpa
10 dpa
smedwi-1 / prog-1 / Hoechst
500µm
C
prog-1
smedwi-1
Distance migrated (µm)
1250
1000
750
500
250
0
1dpa
4dpa
7dpa
10dpa
D
smedwi-1 to prog-1 ratio
3
2
1
0
1dpa
4dpa
7dpa
10dpa
Shielded region
Unexposed
E
H3P
smedwi-1
Number of cells in migratory region
800
600
400
200
0
1dpa
4dpa
7dpa
10dpa

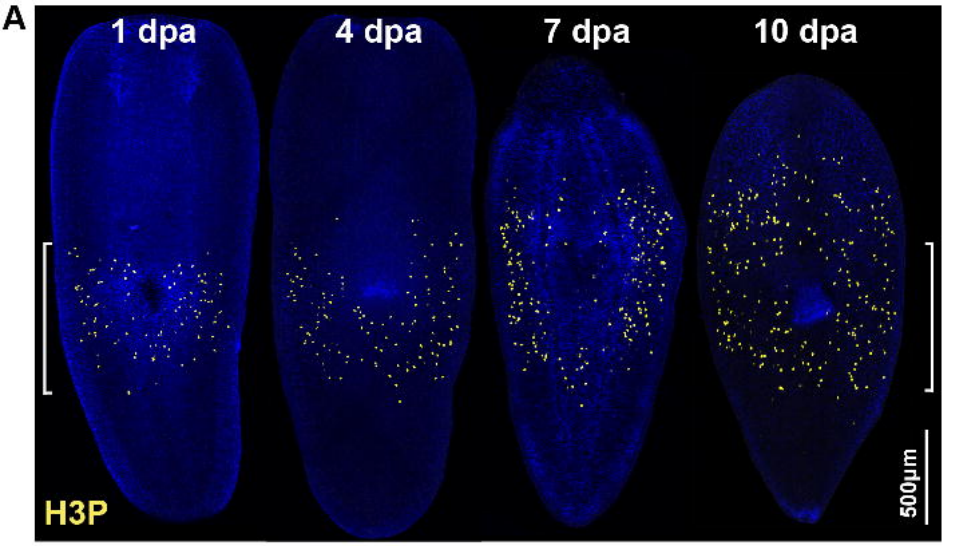
A
1 dpa
4 dpa
7 dpa
10 dpa
H3P
500µm

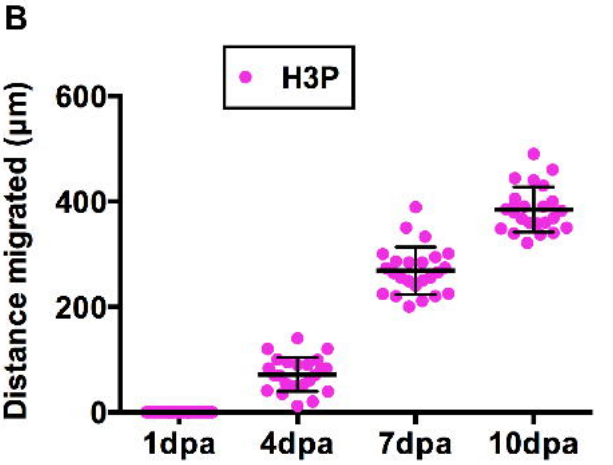
B
H3P
Distance migrated (µm)
600
400
200
0
1dpa
4dpa
7dpa
10dpa

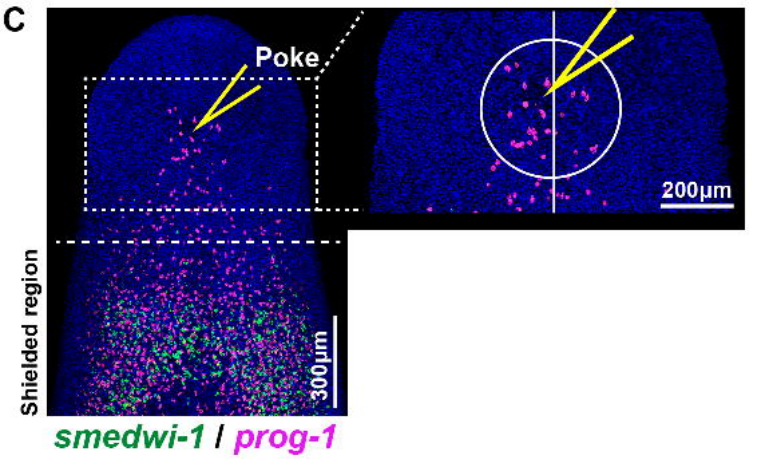
C
Poke
200µm
Shielded region
300µm
smedwi-1 / prog-1

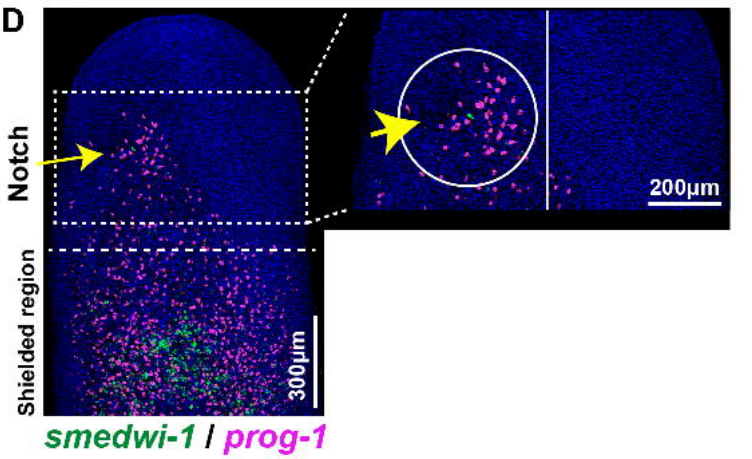
D
Notch
200µm
Shielded region
300µm
smedwi-1 / prog-1

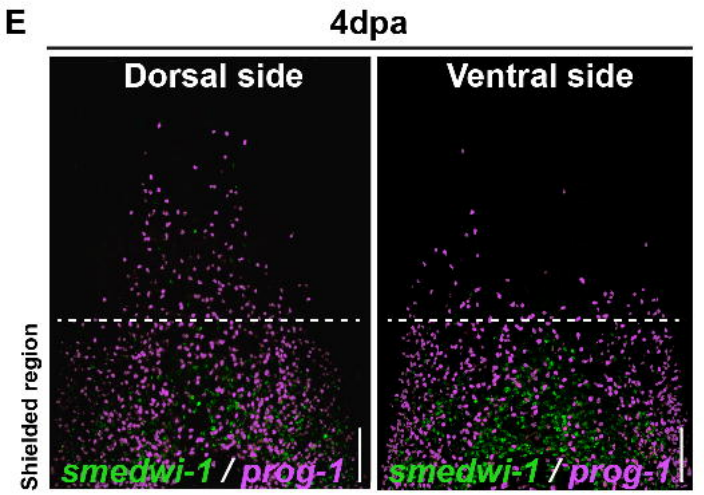
E
4dpa
Dorsal side
Ventral side
Shielded region
smedwi-1 / prog-1
smedwi-1 / prog-1

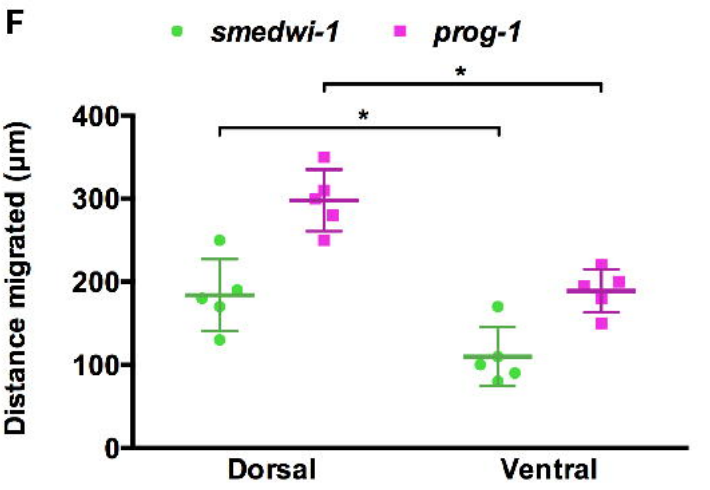
F
smedwi-1
prog-1
*
*
Distance migrated (µm)
400
300
200
100
0
Dorsal
Ventral

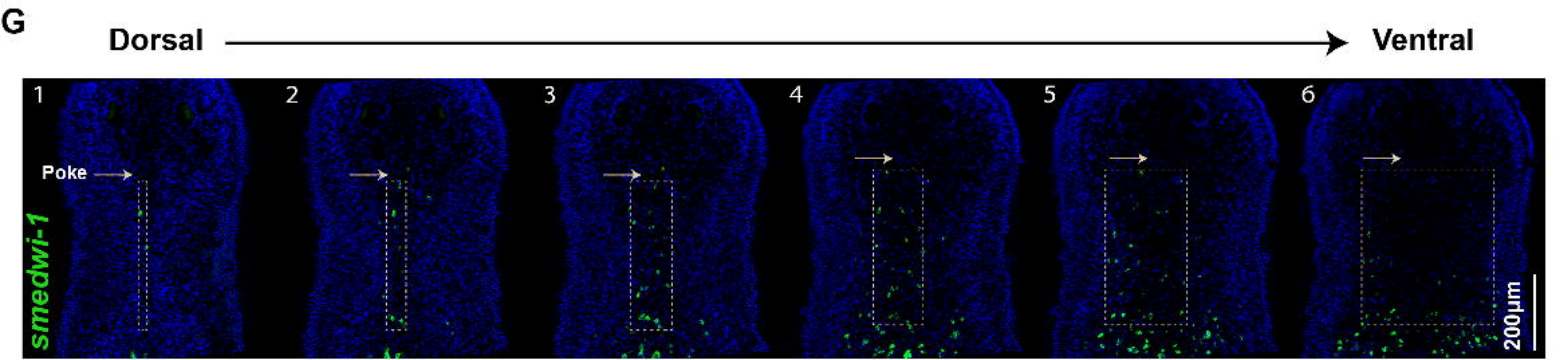
G
Dorsal
Ventral
1
2
3
4
5
6
Poke
smedwi-1
200µm

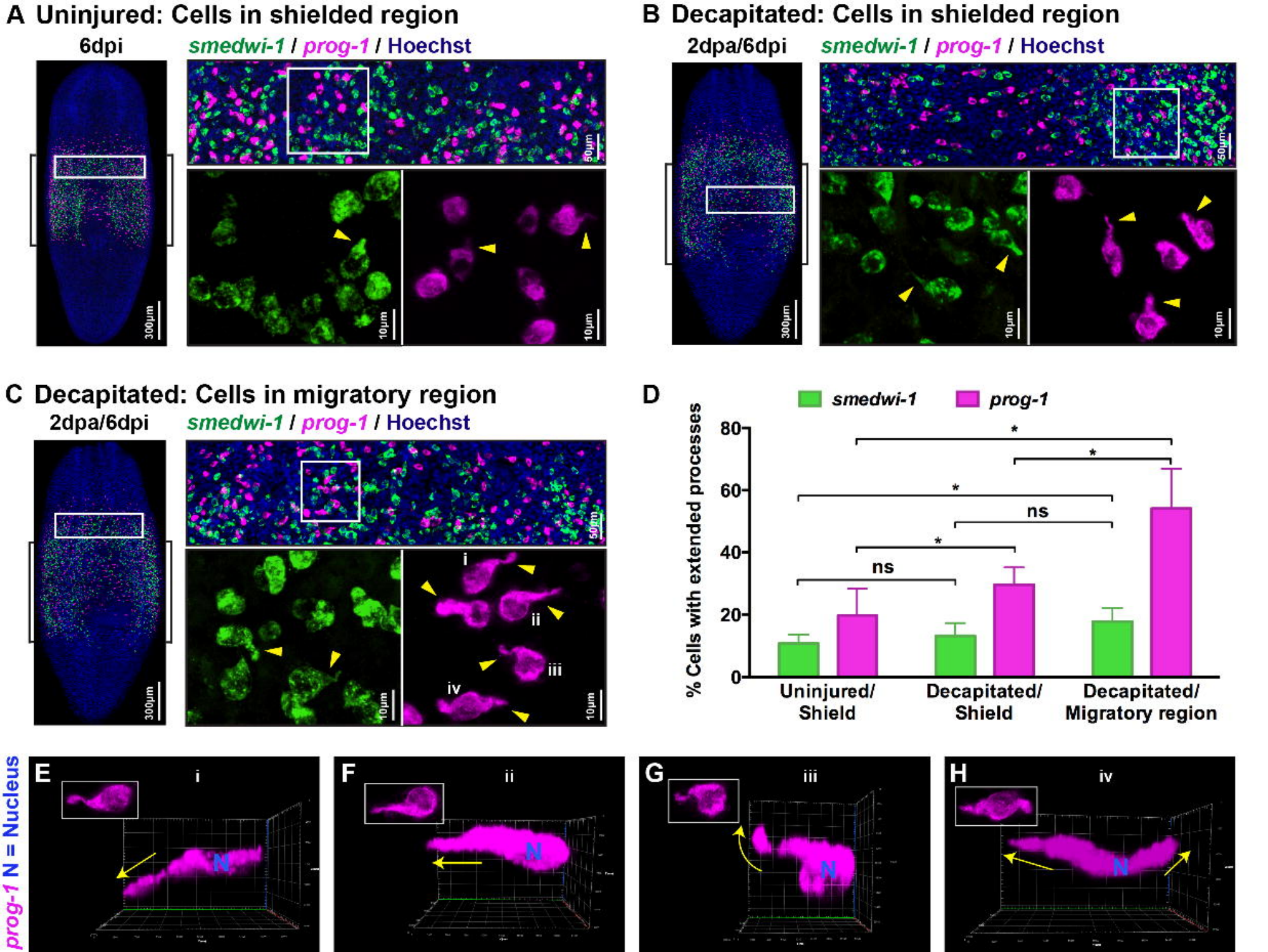
A Uninjured: Cells in shielded region
6dpi
smedwi-1 / prog-1 / Hoechst
300µm
50µm
10µm
B Decapitated: Cells in shielded region
2dpa/6dpi
smedwi-1 / prog-1 / Hoechst
C Decapitated: Cells in migratory region
2dpa/6dpi
smedwi-1 / prog-1 / Hoechst
i
ii
iii
iv
D
smedwi-1
prog-1
% Cells with extended processes
0
20
40
60
80
ns
*
Uninjured/ Shield
Decapitated/ Shield
Decapitated/ Migratory region
E
F
G
H
N
prog-1 N = Nucleus

A

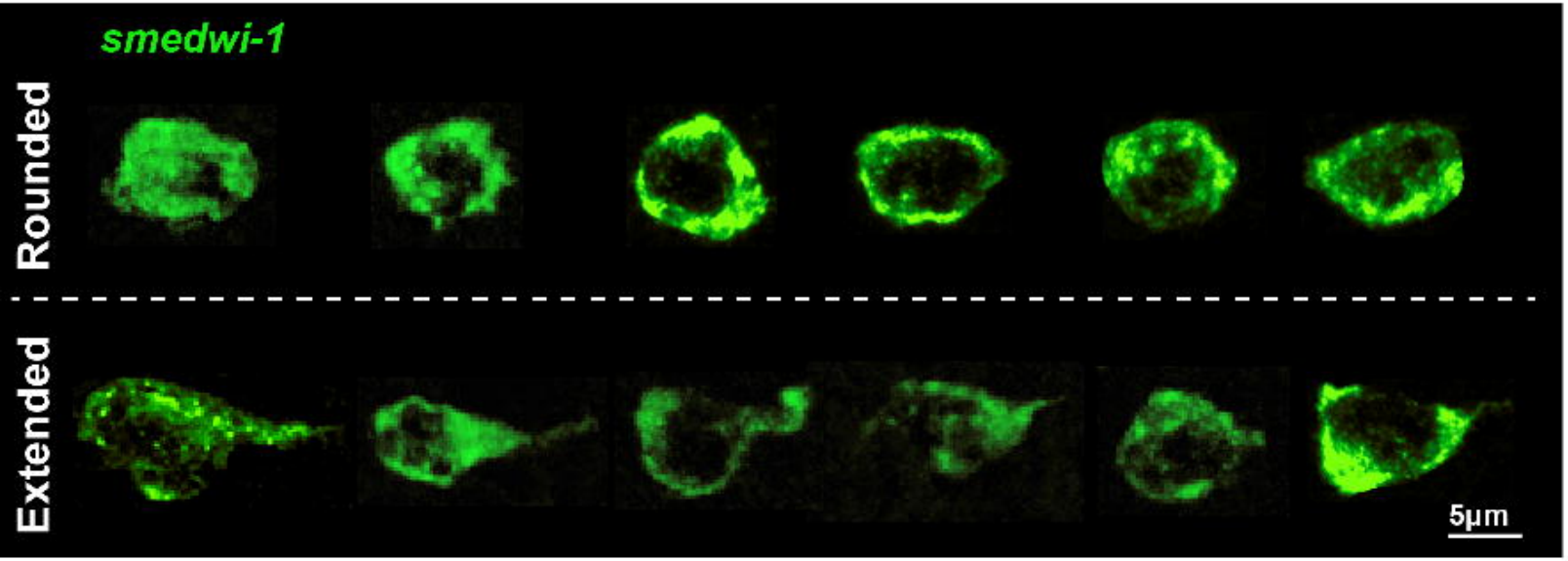

B

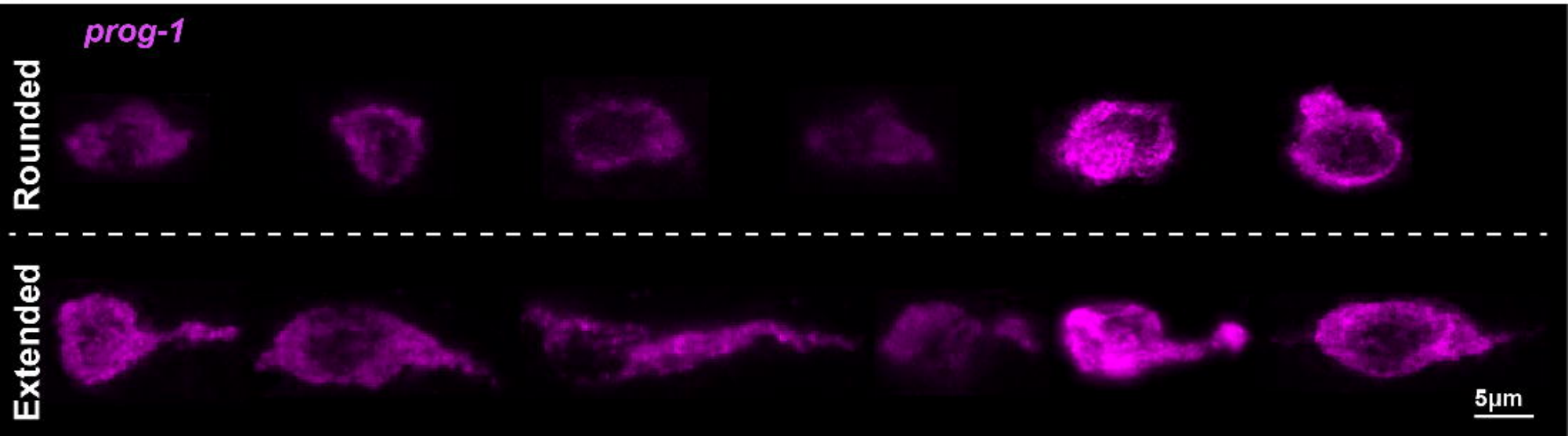

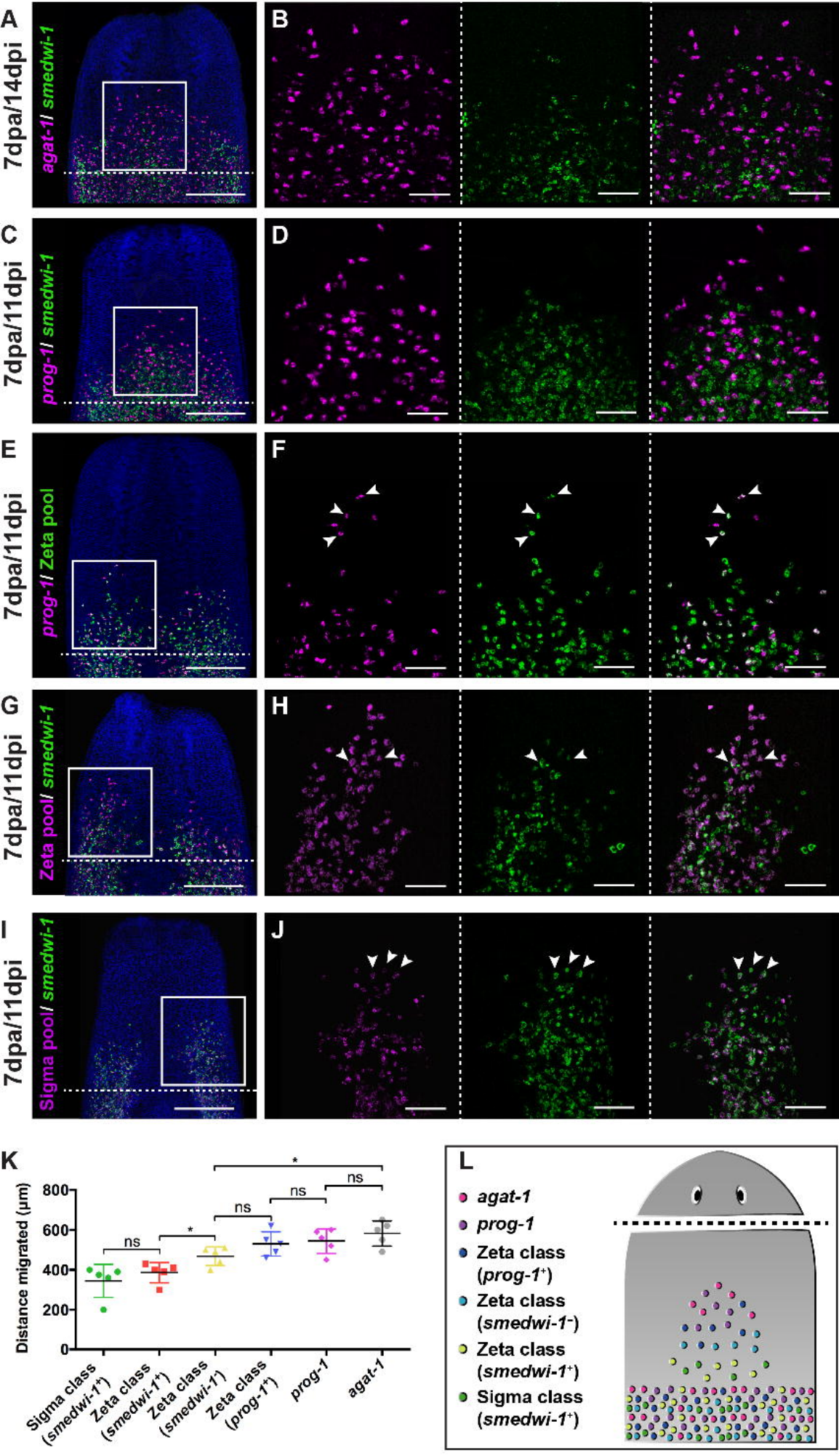
A
7dpa/14dpi
agat-1/ smedwi-1
B
C
7dpa/11dpi
prog-1/ smedwi-1
D
E
7dpa/11dpi
prog-1/ Zeta pool
F
G
7dpa/11dpi
Zeta pool/ smedwi-1
H
I
7dpa/11dpi
Sigma pool/ smedwi-1
J
K
Distance migrated (µm)
800
600
400
200
0
ns
*
ns
ns
ns
*
Sigma class (smedwi-1+)
Zeta class (smedwi-1+)
Zeta class (smedwi-1-)
Zeta class (prog-1+)
prog-1
agat-1
L
agat-1
prog-1
Zeta class (prog-1+)
Zeta class (smedwi-1-)
Zeta class (smedwi-1+)
Sigma class (smedwi-1+)

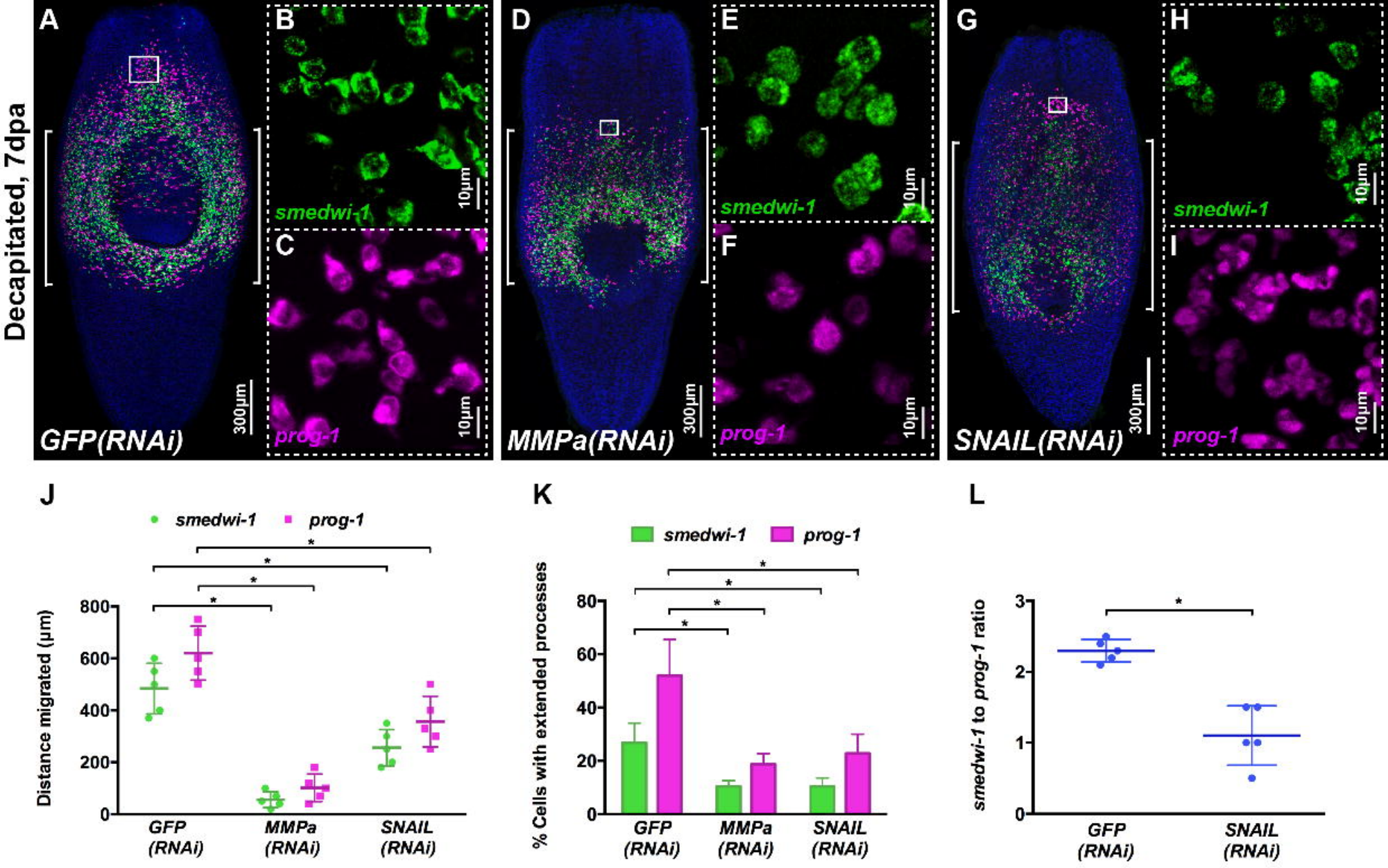
Decapitated, 7dpa
A
B
C
D
E
F
G
H
I
smedwi-1
prog-1
10µm
300µm
GFP(RNAi)
MMPa(RNAi)
SNAIL(RNAi)
J
K
L
smedwi-1
prog-1
Distance migrated (µm)
% Cells with extended processes
smedwi-1 to prog-1 ratio
GFP (RNAi)
MMPa (RNAi)
SNAIL (RNAi)
*

A Regeneration at 11dpa

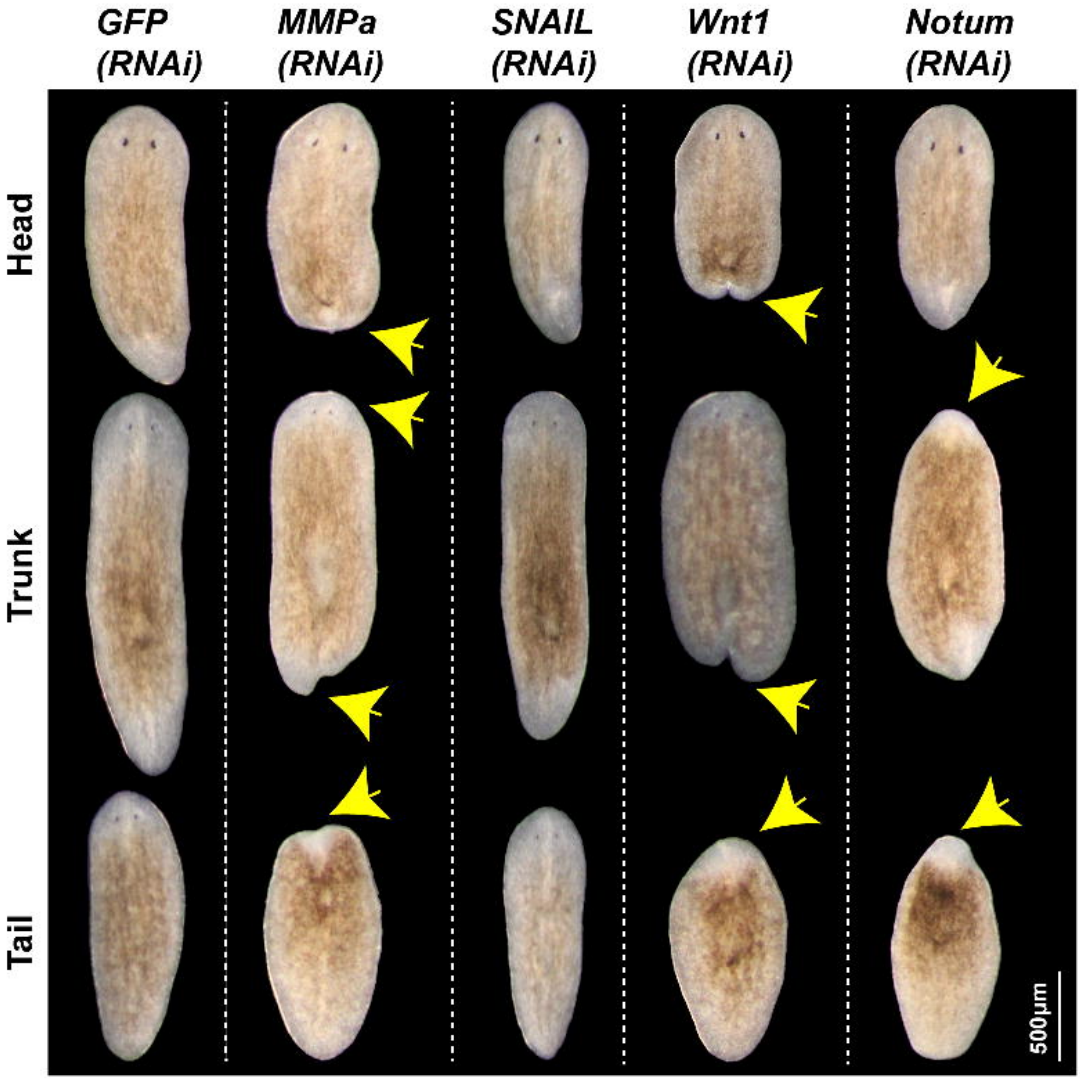

B Regeneration in shielded irradiation assay

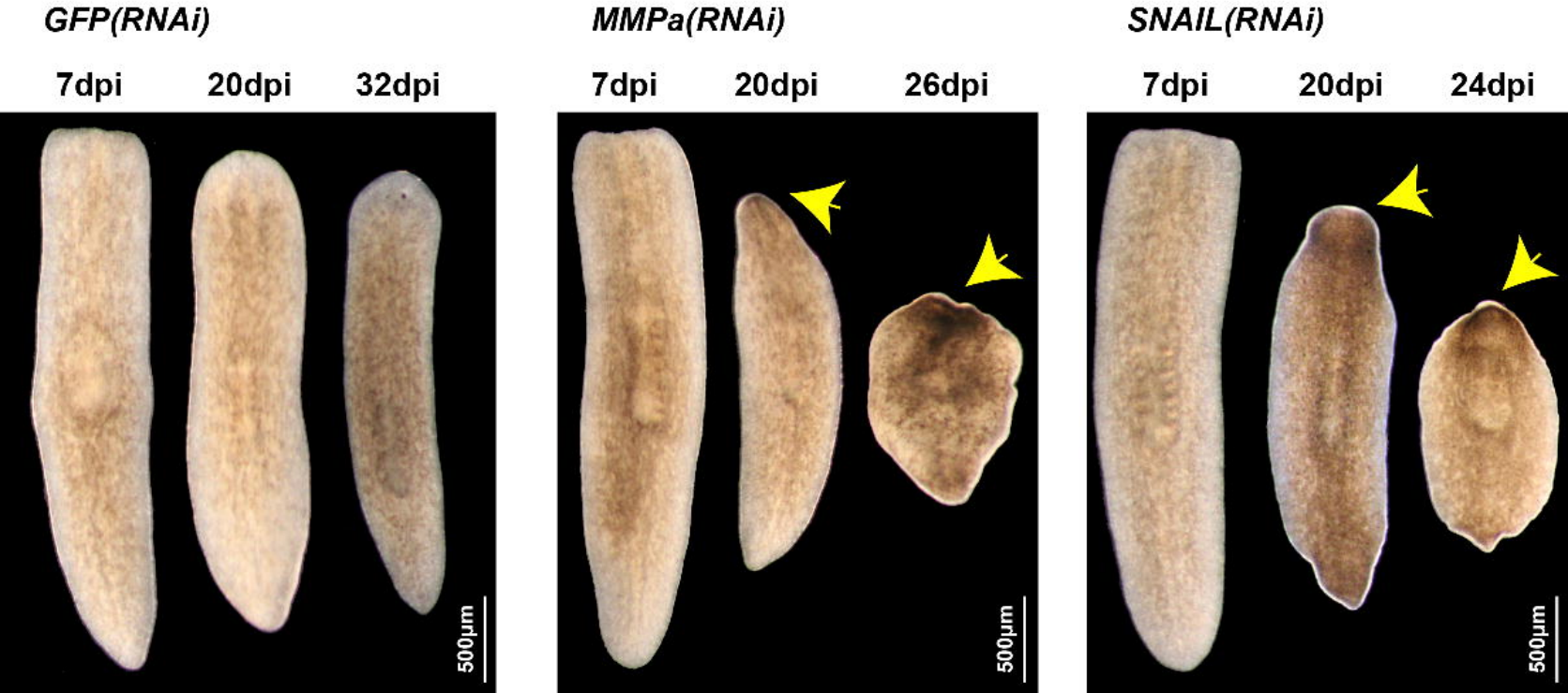

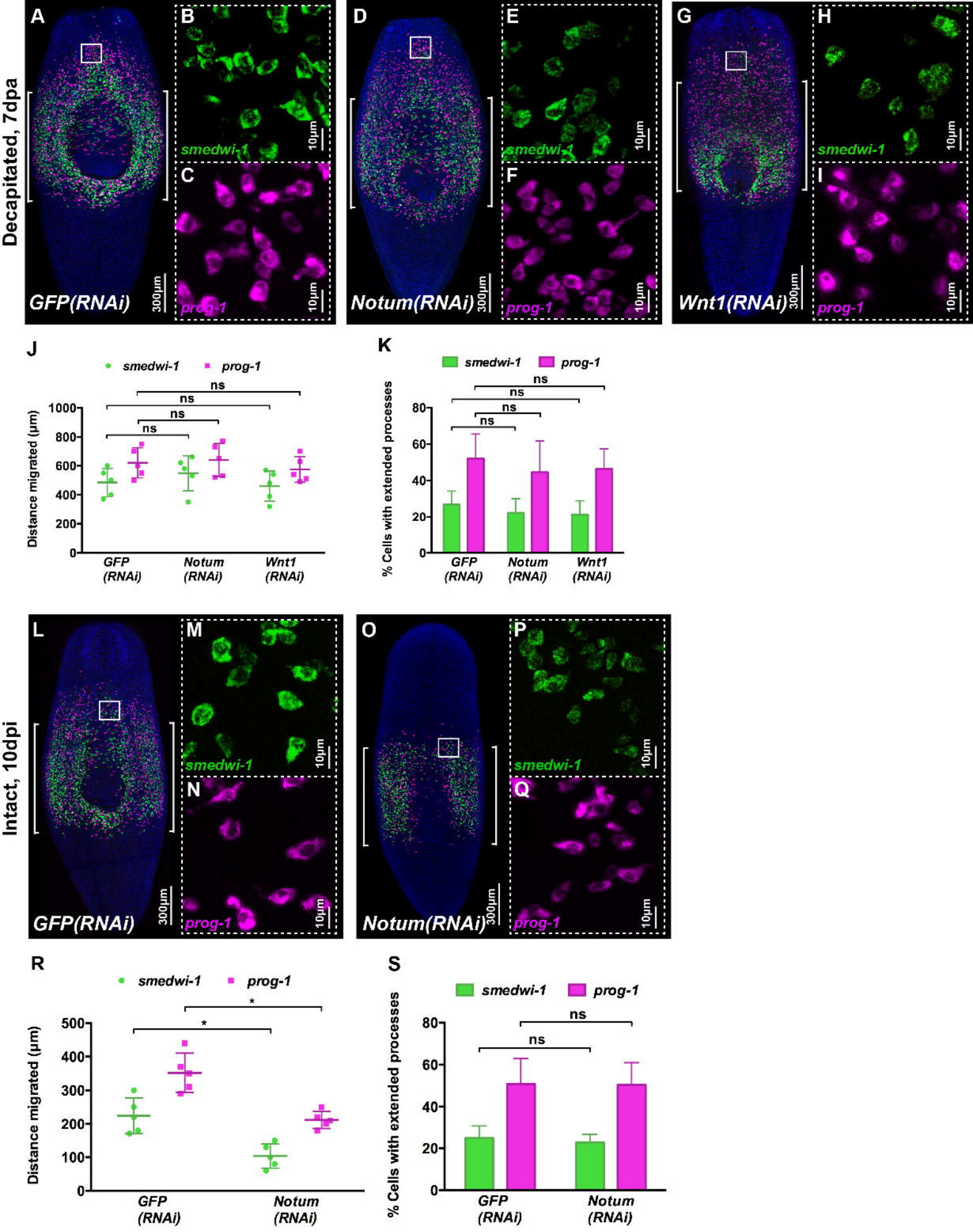
Decapitated, 7dpa
A
B
C
D
E
F
G
H
I
smedwi-1
prog-1
GFP(RNAi)
Notum(RNAi)
Wnt1(RNAi)
300µm
10µm
J
smedwi-1
prog-1
Distance migrated (µm)
ns
GFP (RNAi)
Notum (RNAi)
Wnt1 (RNAi)
K
% Cells with extended processes
Intact, 10dpi
L
M
N
O
P
Q
R
Distance migrated (µm)
*
S
% Cells with extended processes